Hydraulic evaluation of Joltech's GyroPTO for wave energy applications

Kramer, Morten Mejlhede; Pecher, Arthur Francois Serge; Guaraldi, Irene; Andersen, Morten Thøtt; Kofoed, Jens Peter

Publication date:
2015

Document Version
Publisher's PDF, also known as Version of record

Hydraulic evaluation of Joltech's GyroPTO for wave energy applications

Morten Mejlhede Kramer

Arthur Pecher

Irene Guaraldi

Morten Thøtt Andersen

Jens Peter Kofoed

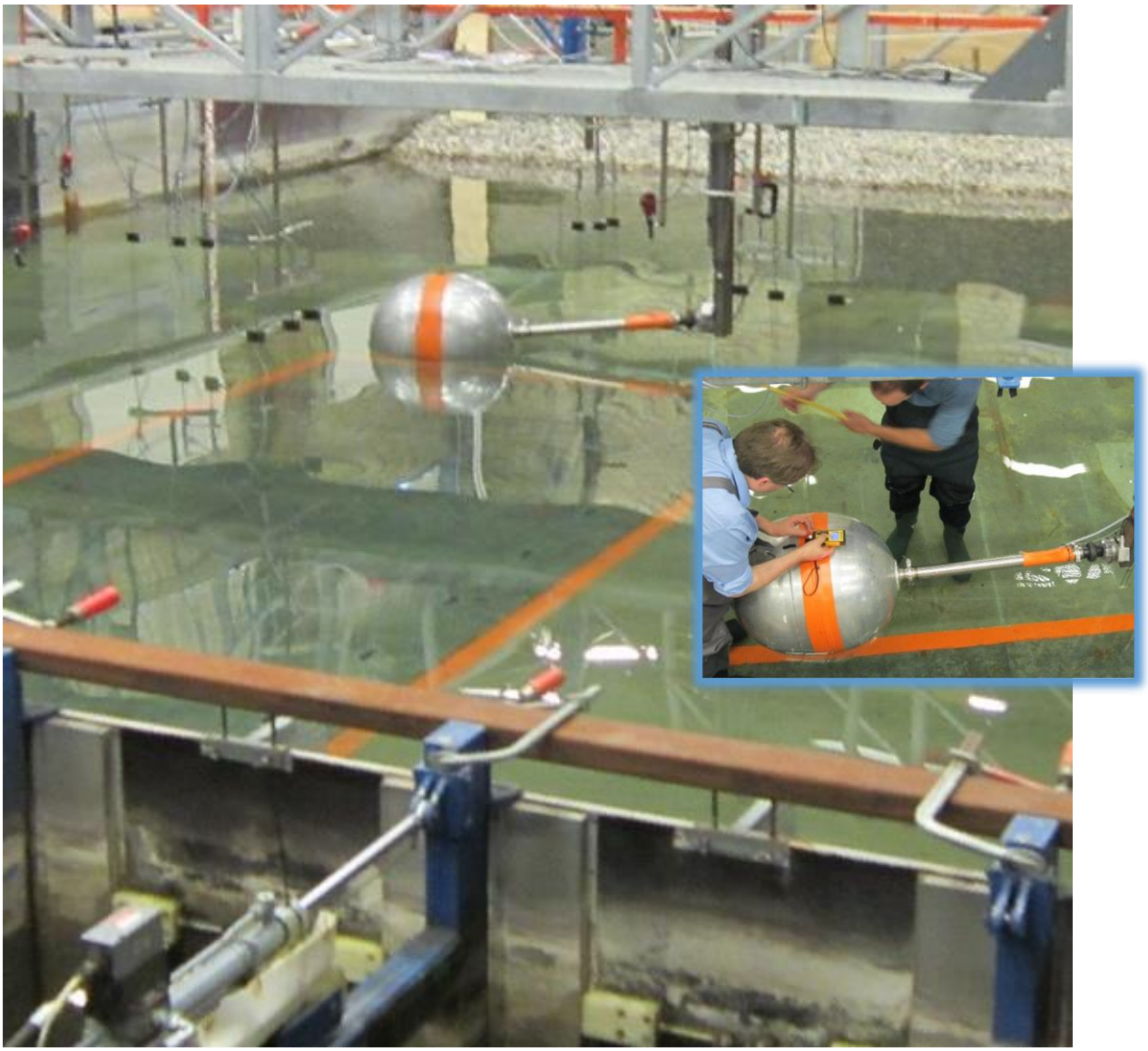

ISSN 1901-726X

DCE Technical Report No. 178

DEPARTMENT OF CIVIL ENGINEERING
AALBORG UNIVERSITY

Aalborg University
Department of Civil Engineering
Wave Energy Research Group

DCE Technical Report No. 178

Hydraulic evaluation of Joltech's GyroPTO for wave energy applications

March 2015

Scientific Publications at the Department of Civil Engineering

Technical Reports are published for timely dissemination of research results and scientific work carried out at the Department of Civil Engineering (DCE) at Aalborg University. This medium allows publication of more detailed explanations and results than typically allowed in scientific journals.

Technical Memoranda are produced to enable the preliminary dissemination of scientific work by the personnel of the DCE where such release is deemed to be appropriate. Documents of this kind may be incomplete or temporary versions of papers—or part of continuing work. This should be kept in mind when references are given to publications of this kind.

Contract Reports are produced to report scientific work carried out under contract. Publications of this kind contain confidential matter and are reserved for the sponsors and the DCE. Therefore, Contract Reports are generally not available for public circulation.

Lecture Notes contain material produced by the lecturers at the DCE for educational purposes. This may be scientific notes, lecture books, example problems or manuals for laboratory work, or computer programs developed at the DCE.

Theses are monograms or collections of papers published to report the scientific work carried out at the DCE to obtain a degree as either PhD or Doctor of Technology. The thesis is publicly available after the defence of the degree.

Latest News is published to enable rapid communication of information about scientific work carried out at the DCE. This includes the status of research projects, developments in the laboratories, information about collaborative work and recent research results.

Published 2015 by
Aalborg University
Department of Civil Engineering
Sohngaardsholmsvej 57,
DK-9000 Aalborg, Denmark

Printed in Aalborg at Aalborg University

ISSN 1901-726X
DCE Technical Report No. 178

Contents

1 Preface

The work presented in this report was completed under the support from the Danish Energy Technological Development and Demonstration Program (EUDP), project no. 64014-0129 "Gyro electric energy converter unit for wave energy".

Testing took place in the wave basin at the Department of Civil Engineering at Aalborg University in the period between Monday 29 September to Friday 10 October 2014. The laboratory activities were carried out by Morten Kramer, Jan Olsen, Irene Guaraldi, Morten Thøtt, and Nikolaj Holk.

Jan Olsen was representative for the Joltech GyroPTO, and Jens Peter Kofoed was coordinating the work by representing Aalborg University.

Jan Olsen
B.Sc., Mech. Eng.
Research & Development

Direct tel.: +45 2330 9617
Email: jao@joltech.dk

Joltech ApS
Nordborgvej 81 E14/S13
6430 Nordborg
CVR nr.: 30 81 29 13

Jens Peter Kofoed
Associate Professor

Phone: 9940 8474
jpk@civil.aau.dk

Department 6 - Department of Civil Engineering
Sofiendalsvej 11
Room: 11-205
9200 Aalborg SV, DK

2 Introduction

The main purpose of the tests was to investigate the power absorption performance in irregular waves, but testing also included performance measures in regular waves and simple tests to get knowledge about characteristics of the device, which could facilitate the possibility of performing numerical simulations and optimisations. The simple tests included measurements of the physical size, weight, inertia moments, hydrostatics, eigen periods, mooring stiffness, friction, hydrodynamic coefficients etc.

The present report includes documentation regarding the power production performance. Several additional measurements were performed which are available in the data files from the experiments.

The GyroPTO (Gyroscopic Power Take-Off) wave energy point absorber is being developed by Joltech. It consists of a float arm rigidly connected to a ball, and the arm is connected to a universal joint attached to the support structure. The system has 3 degrees of freedom. Twisting torque of the arm is fixed in the joint but the joint allows the device freely to perform rotations around two axes. The motion of the ball is described by the two degrees of freedom:

- Roll, φ. Rotation about the horizontal x-axis (wave propagation direction) caused by the vertical motion of the ball
- Yaw, θ. Rotation about the vertical z-axis caused by the horizontal motion of the ball

In addition to the above the ball has a single internal degree of freedom which couples the internal motions (generator, flywheel and outer ring) to the ball and arm motion:

- Rotation of flywheel, α.

Figure 1. Overview of lab-model.

The PTO consists of the following main components:

- A 90 W 24 V Maxon EC 90 Brushless DC motor
- A 4Q Maxon DECV 50/5 brushless DC Motor controller
- CompactRIO controller from National Instruments

3 Scaling

The scaling is performed using the so-called Froude scaling, assuming the forces involved are dominated by inertia. The length is used as basis for the scaling ratio *n*. As the laboratory model is not exactly a sphere in shape, the scale is calculated from the float volume *V* by: $n = (V/V_{lab})^{\wedge 1/3}$. This ratio has been used in Table 1, where it is for example seen that the Nissum Bredning device with Ø1.5 m float is a scale 1:2.57 of the laboratory model. The indicated power ratings have been chosen just for indications, and they does not match exactly the scaling criteria.

Table 1. Scale relative to the lab device of the Nissum Bredning device and a hypothetical North Sea device.

Parameter	**Laboratory model**	**Nissum Breding**	**North Sea**
Float size (m)	0.630*0.550	Ø 1.5	Ø 5
Float volume (m^3)	0.104	1.77	65.4
Scale relative to lab	1	2.57	8.57
Power rating	90 W	5 kW	250 kW

When using Froude scaling the following applies:

Length	n
Time	$n^{0.5}$
Velocity	$n^{0.5}$
Force	n^3
Power	$n^{3.5}$

4 Geometry, weight and static position

The ball is composed by two hemispheres (R = 270 mm) connected by a 90 mm slightly wider cylinder (R = 275 mm). The connection piece is made such that the two ball parts can be taken apart to gain access to the PTO inside the ball, see Figure 2. In Figure 3 detailed measures are given, i.e. the ball centre is located 1054 mm from the rotation centre and the rotation centre is 150 mm above the water level.

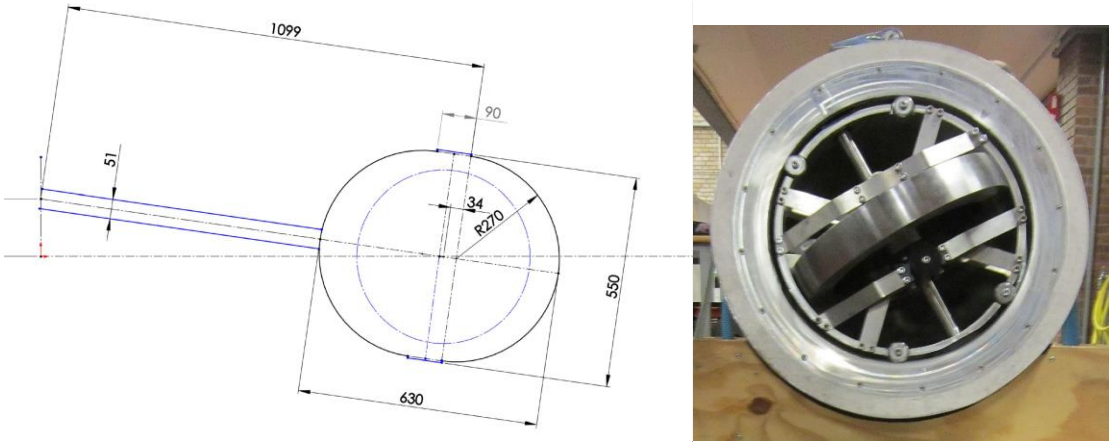

Figure 2. Overview of geometry of lab-model.

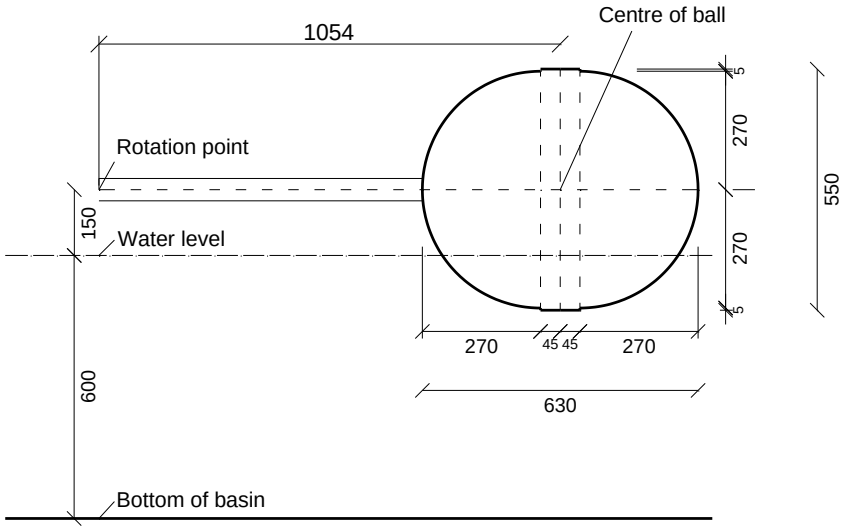

Figure 3. Details of geometry of lab-model, horizontal position before submergence in water.

The ball is lowered into the water by a rotation around the bearing. When submerged at static equilibrium the buoyancy force is balanced by the gravity force, and the angle of rotation is -7.1°, see Figure 4.

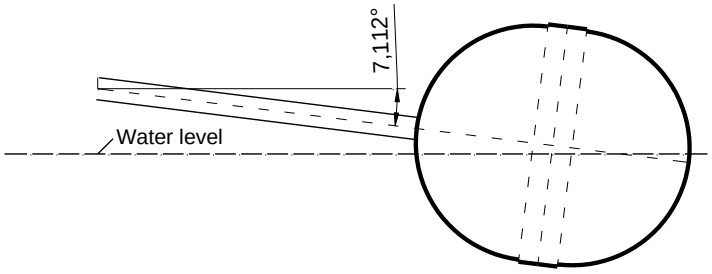

Figure 4. Details of geometry of lab-model, position at rest in calm water.

The weight of the device was measured to be 47.0 kg, see Figure 5.

Figure 5: Measured weight of the device

The inclination of the device when placed in calm water with the PTO turned off was measured to be about -7.0°, see Figure 6.

Figure 6: Measured inclination of the device at rest in calm water.

5 Laboratory set up

The device was placed approximately in the middle of the basin, perpendicular to the direction of the waves and attached to the bridge from above the water, see Figure 7.

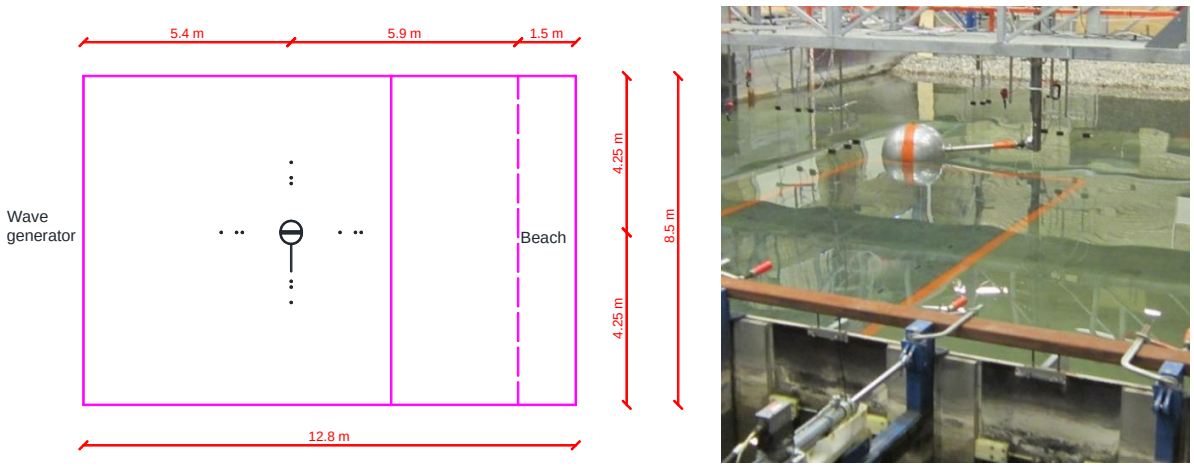

Figure 7: Overview of the basin. The dashed line indicates the water level at the beach.

5.1 Position of WG´S

A total of 12 wave gauges were placed on the four sides of the device with 3 sensors at each side, see Figure 8. The distance from the centre of the float to the closest wave gauge was 127 cm.

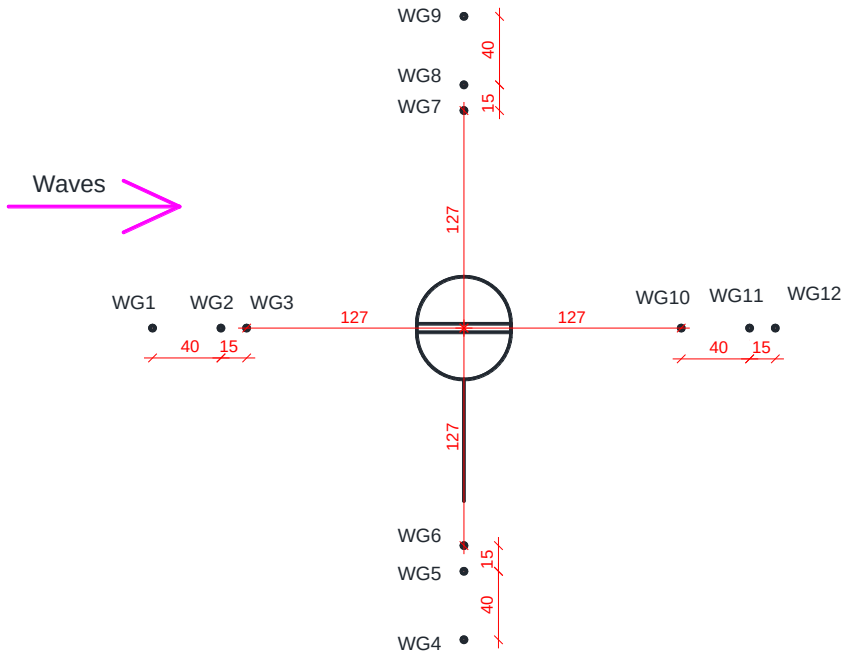

Figure 8: Position of the 12 Wave Gauges. Measures in cm.

5.2 Mooring lines and mooring force sensors

In order to keep the device in the zero position two mooring lines were attached to the device. The mooring lines provided the necessary stiffness restricting yaw motions. The lines were 2.5 m each and mooring line 1 headed towards the wave generator and mooring line 2 headed towards the beach. The lines were almost horizontal and pre-tensioned, and a force sensor was placed in each line, see Figure 9.

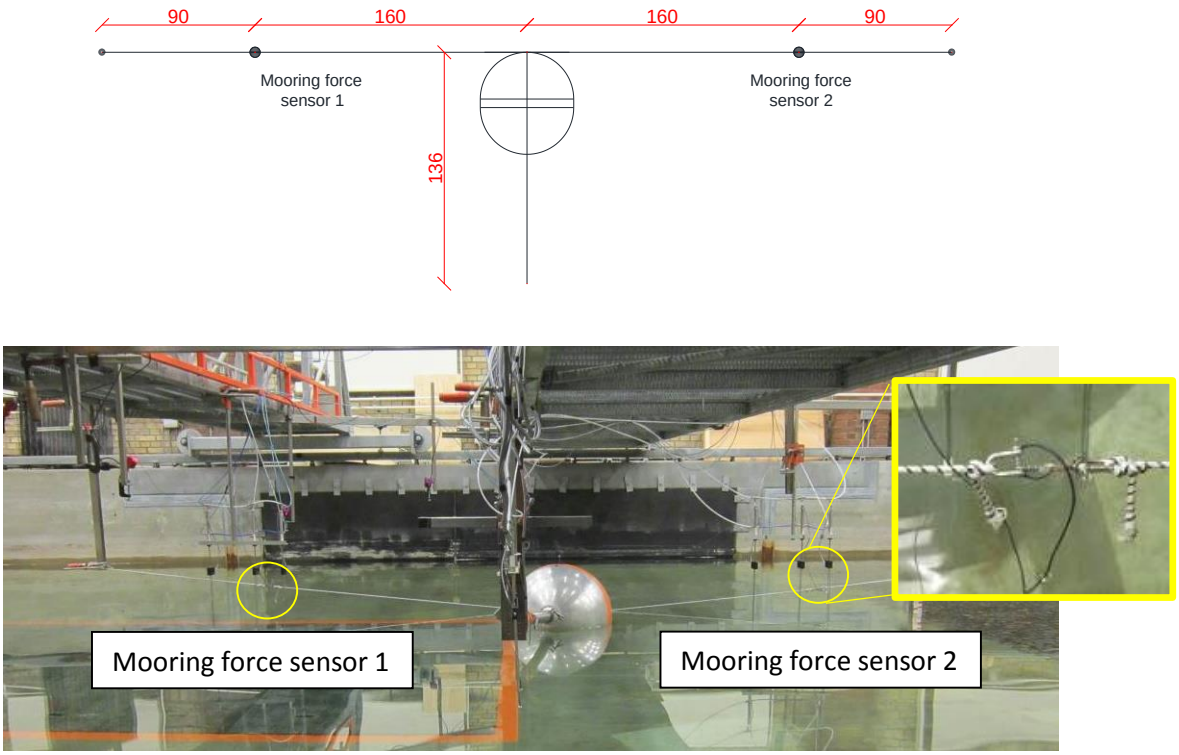

Figure 9: Mooring lines and mooring force sensor positions. A zoom on a force sensor is shown. Position measures in cm.

5.3 Reaction point force measurements

A six axis force sensor was placed at the point where the arm was attached the support, see Figure 10. All 6 components of the forces (Fx, Fy and Fz) and moments (Mx, My, Mz) were measured.

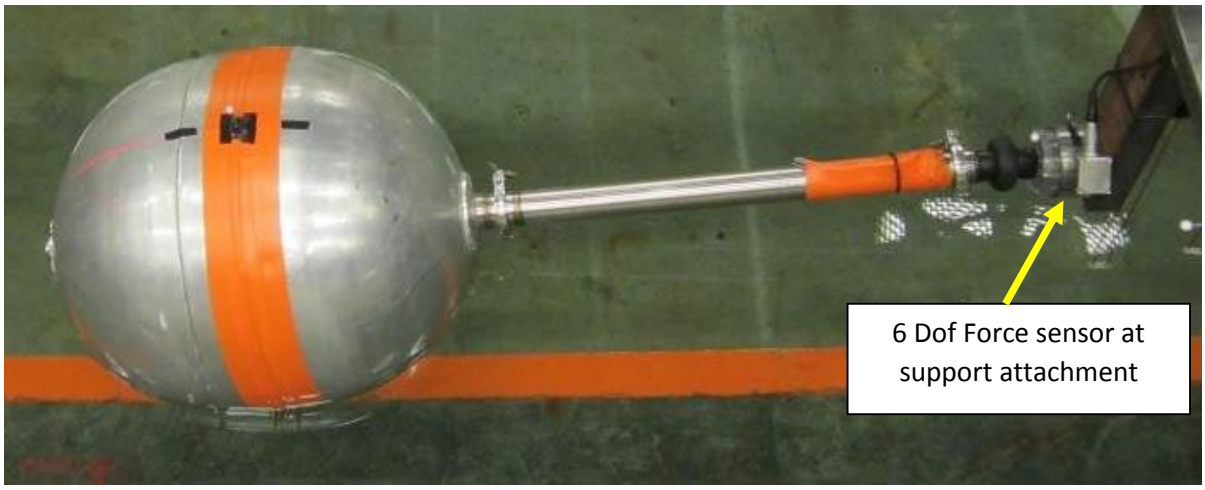

Figure 10: Six-dof force sensor.

5.4 Position tracking

A 3D Video tracking system was used to track the position of the ball motion. 4 cameras and 4 markers were used, see Figure 11. Marker number 1 was placed on top of the floats and it followed the float motions. Marker number 2, 3 and 4 were placed at fixed static positions for reference, and they did not move.

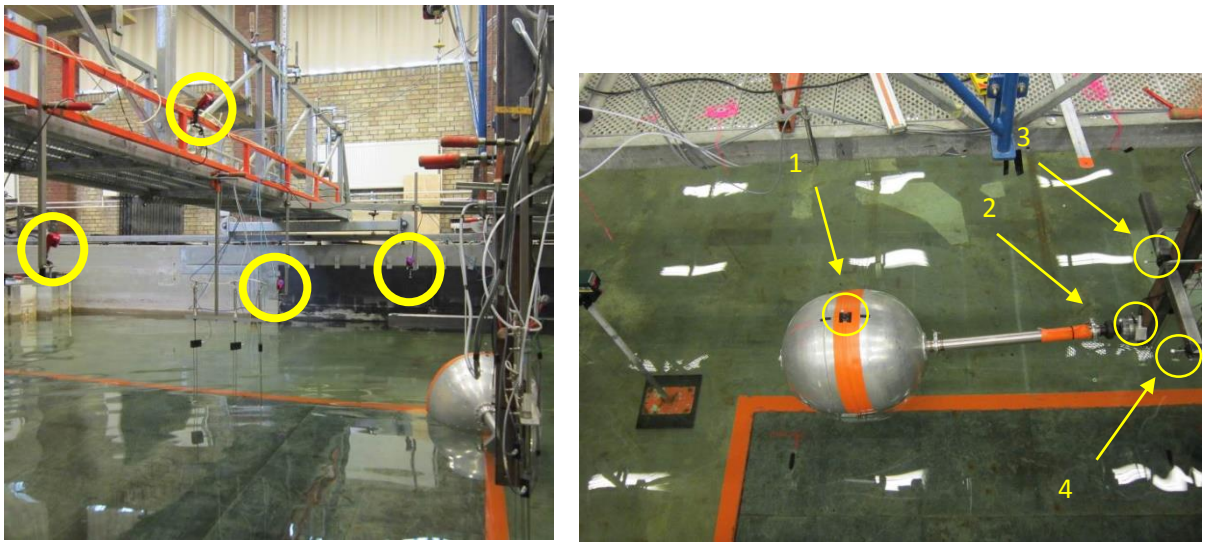

Figure 11: Position of the 4 cameras for position tracking (left), and position of the four markers (right).

5.5 Video

A webcam was installed to record video during experiments, see Figure 12. Synchronization was performed using a LED-lamp which was lighted by the trigger-signal.

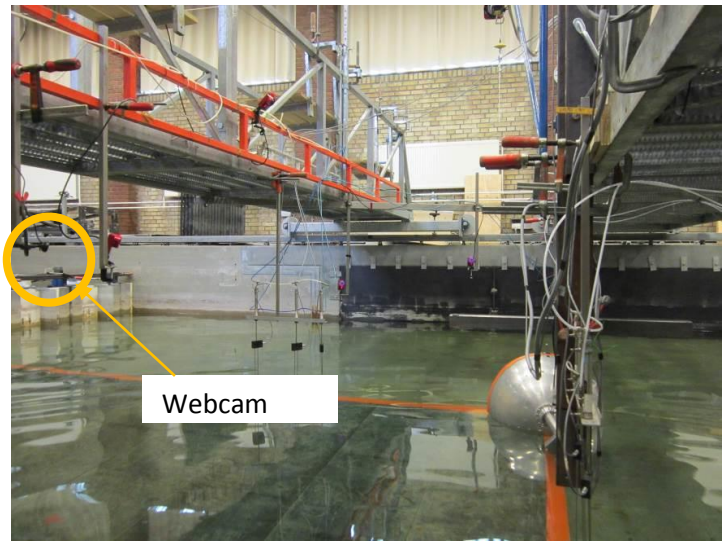

Figure 12: Position of the webcam used for video recordings.

6 Coordinate systems

Three coordinate systems were used:

1) {G}, a global system with origo at the bearing. The x-axis is in the wave direction and the z-axis is upward. The system is shown in Figure 13.
2) {C}, the camera coordinate system with origo at the position of marker 3. The z-axis is pointing towards the waves and the x-axis is pointing upwards.
3) {F}, the six-axis force sensor coordinate system with origo at the arm mount (close to the bearing). The x-axis is pointing downwards, and the y-axis is pointing towards the waves.

The motion of the device is described in a global coordinate system with origo located at the centre of the arm bearing. Waves are propagating in the direction of the x_G-axis, see Figure 13 and Figure 14.

Panoramic view

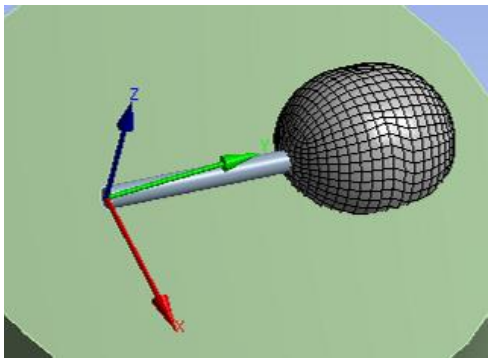

View from the side

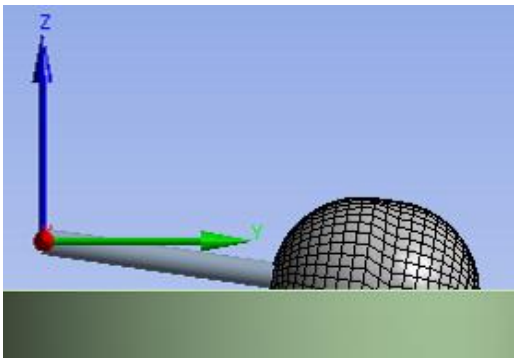

View from above

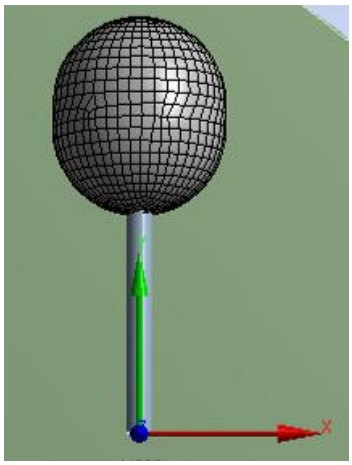

View from behind

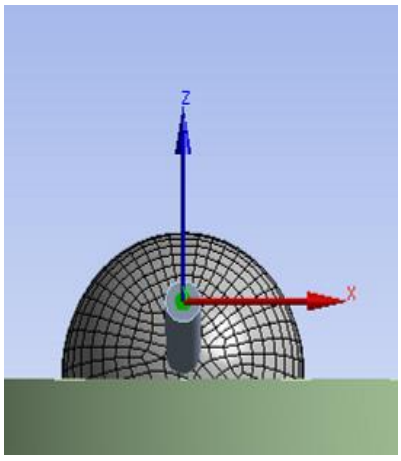

Figure 13: Global coordinate system

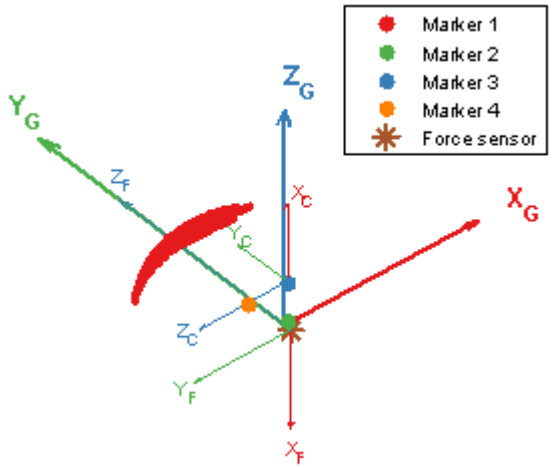

X_G, Y_G, Z_G : Global system

X_C, Y_C, Z_C : Camera system

X_F, Y_F, Z_F : Force system

Figure 14: Coordinate systems and example data with position tracking of marker 1.

Details are given in the following tables.

Table 2: Camera coordinate system axes.

Global coordinate system axes	Camera coordinate system
X_G	Z_C
Y_G	Y_C
Z_G	$-X_C$

Table 3: Marker positions. Position of marker 1 is given at mean position.

Marker number	X_C (m)	Y_C (m)	Z_C (m)
1 (on float)	*0.235*	*1.09*	*0*
2	*0.357*	*0*	*0*
3	*0*	*0*	*0*
4	*0*	*0*	*-0.359*

Table 4: Force sensor coordinate system.

Global system	Force sensor
$F_{X,G}$	$-F_{Y,F}$
$F_{Y,G}$	$F_{Z,F}$
$F_{Z,G}$	$-F_{X,F}$
$M_{X,G}$	$-M_{Y,F}$
$M_{Y,G}$	$M_{Z,F}$
$M_{Z,G}$	$-M_{X,F}$

Table 5: Force sensor position.

X_G (m)	Y_G (m)	Z_G (m)
0	*-0.068*	*0*

7 Datalogging

Four computers were used to generate the waves and measure the performance, see Figure 15. The wavegenerator software was providing the trigger signal, which was recorded by the tree other systems.

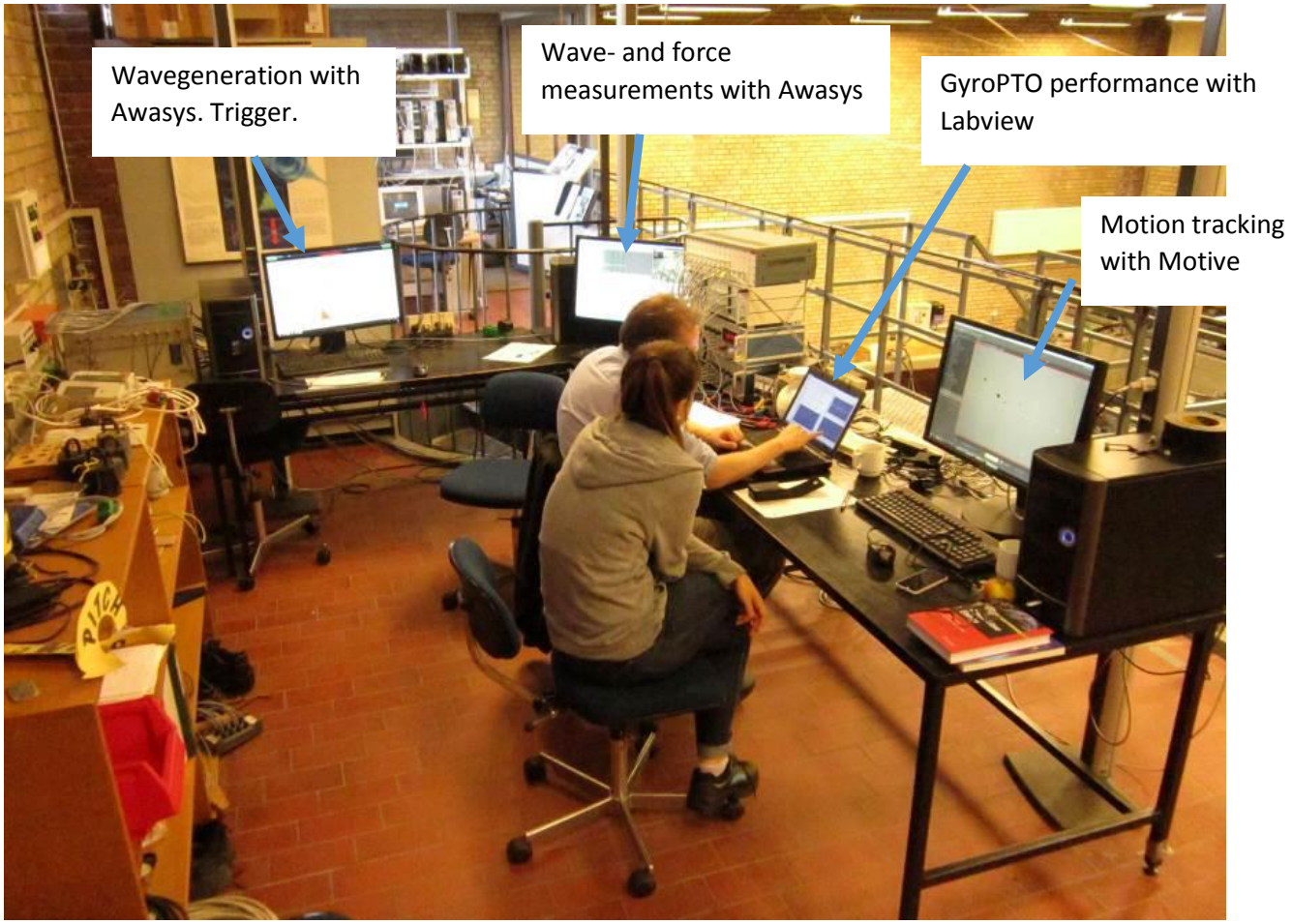

Figure 15. Data was managed on 4 computers from the control room at the balcony above the wave basin.

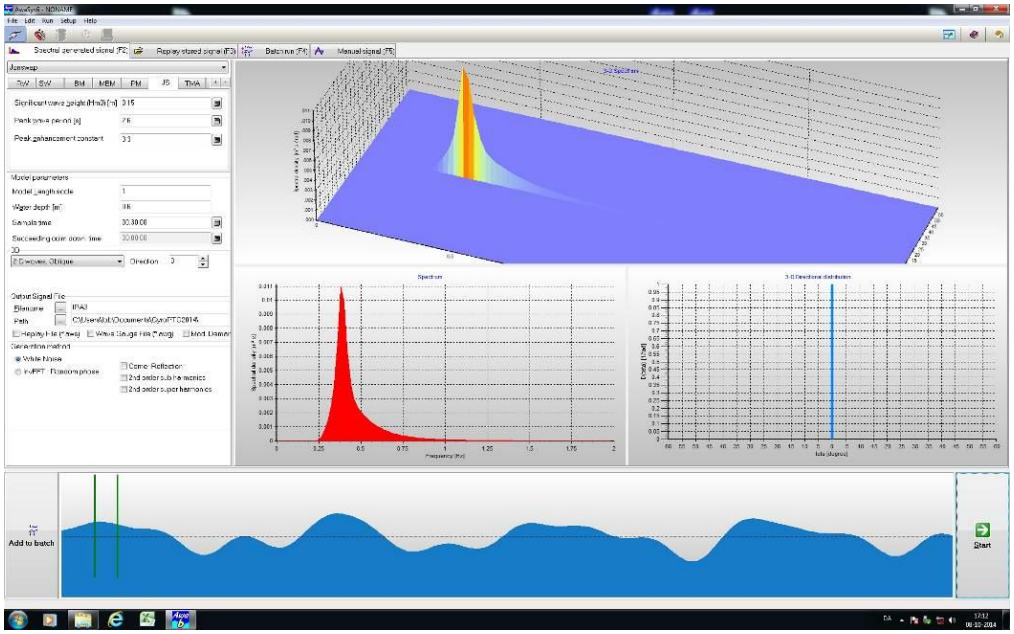

Figure 16. Screendump from Awasys which generated the waves.

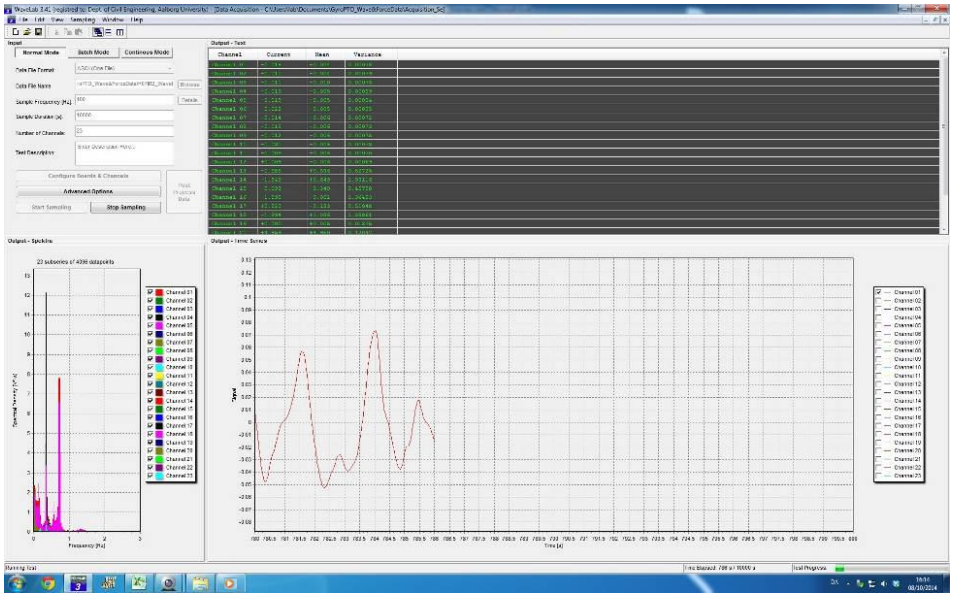

Figure 17. Screendump from Wavelab measuring the waves and forces.

Figure 18. Screendump from Labview measuring the device performance.

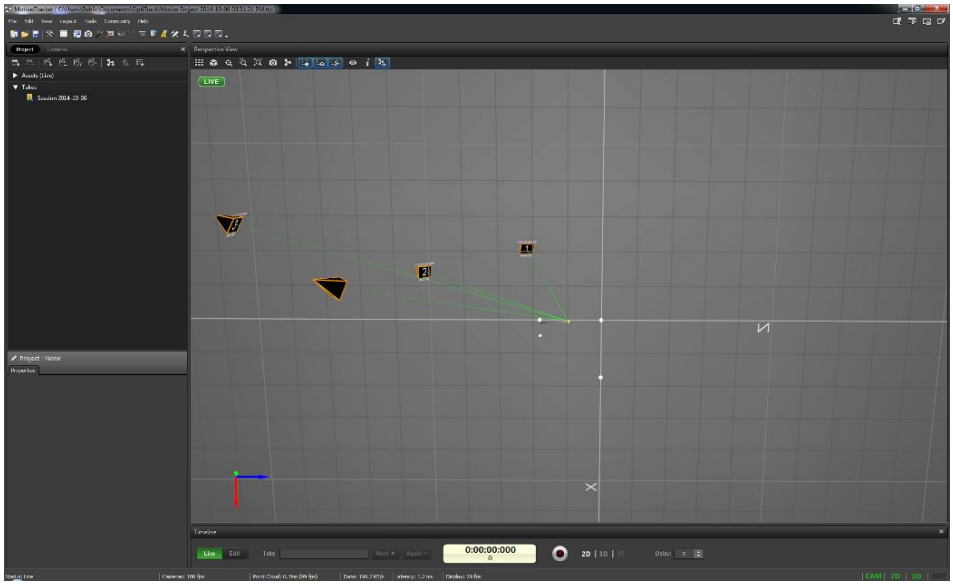

Figure 19. Screendump from Motive which recorded the motion of the device.

7.1 Datafiles

Data were stored from 3 systems:

- "WL" is from the WaveLab-system.
- "PTO" is from the Power Take Off Labview-system
- "OT" is from OptiTrack, Motive-system

The original files are stored in Ascii-text format. Some channels are calibrated, while others are not. Time is not syncronised in the original files, but the trigger signal is included.

To enable easy interpretation and access, bundled and synchronised files has been generated for easy use in Matlab. The bundled files contain a single data-structure for each test, with calibrated and synchronised data. Both file-information (original filename, date- and time stamp) and data are stored. Contents are described in Figure 20.

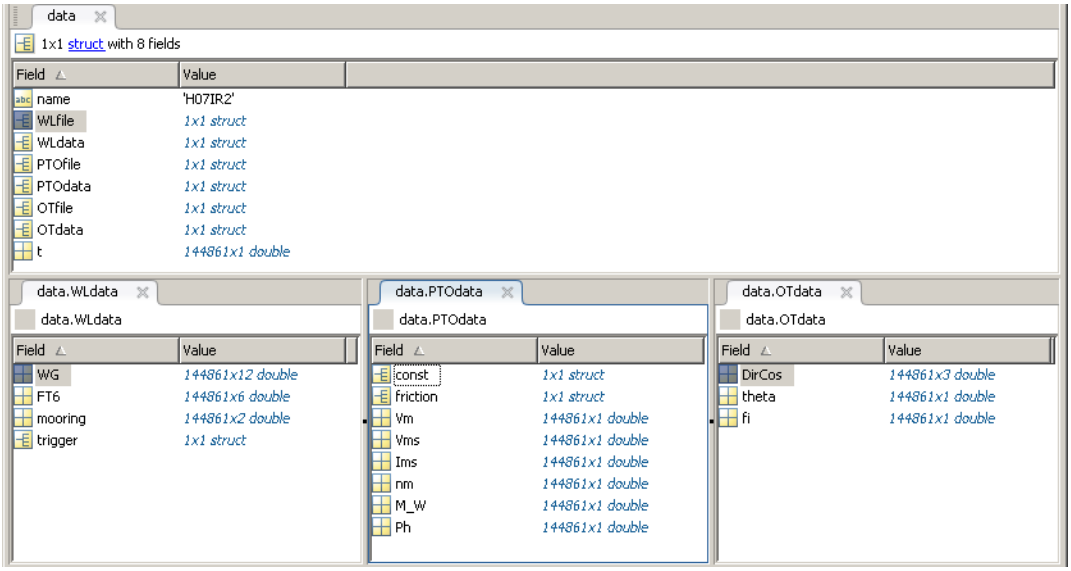

Figure 20. Contents of bundled files in Matlab. Contents of data-structures are shown.

Table 6. Contents of original PTO-datafile.

_PTO		
Channel	**Contents**	**unit**
1	Time starting from year 1900	s
2	Motor current	A
3	Speed set for motor controller	[0 - 5 V]
4	Current set. Current limit on controller, always 5 V (how fast can the wheel be	V
5	Wave period. Manual setting	s
6	Wave height. Manual setting	m
7	Wheel freq. 100 pulses per rotation	[pulses/s]

Table 7. Contents of original WaveLab-datafile.

_WaveLab		
Channel	**Contents**	**unit**
1	Time	s
2	Wave Gauge 1	m
3	Wave Gauge 2	m
4	Wave Gauge 3	m
5	Wave Gauge 4	m
6	Wave Gauge 5	m
7	Wave Gauge 6	m
8	Wave Gauge 7	m
9	Wave Gauge 8	m
10	Wave Gauge 9	m
11	Wave Gauge 10	m
12	Wave Gauge 11	m
13	Wave Gauge 12	m
14	FT6-SG0	V
15	FT6-SG1	V
16	FT6-SG2	V
17	FT6-SG3	V
18	FT6-SG4	V
19	FT6-SG5	V
20	Trigger Wave (Awasys)	V
21	Trigger PTO (Jan Olsen system)	V
22	Trigger Video (Position tracking system)	V
23	Mooring line 1 (closest to wave generator)	N
24	Mooring line 2 (closest to beach)	N

Table 8. Contents of original Optitrack-datafile.

_OptiTrack		
Channel	**Contents**	**unit**
3	time	s
6	Marker 1 (unknown order), x-position (Optitrack coordinate system)	m
7	Marker 1 (unknown order), y-position (Optitrack coordinate system)	m
8	Marker 1 (unknown order), z-position (Optitrack coordinate system)	m
11	Marker 2 (unknown order), x-position (Optitrack coordinate system)	m
12	Marker 2 (unknown order), y-position (Optitrack coordinate system)	m
13	Marker 2 (unknown order), z-position (Optitrack coordinate system)	m
16	Marker 3 (unknown order), x-position (Optitrack coordinate system)	m
17	Marker 3 (unknown order), y-position (Optitrack coordinate system)	m
18	Marker 3 (unknown order), z-position (Optitrack coordinate system)	m
21	Marker 4 (unknown order), x-position (Optitrack coordinate system)	m
22	Marker 4 (unknown order), y-position (Optitrack coordinate system)	m
23	Marker 4 (unknown order), z-position (Optitrack coordinate system)	m

8 Test schedule

Tests were performed during two weeks and the days during the 10 weekdays were given the labelling letters A-J, see Table 9. The labelling was used for the file-names.

Details about the testing is given in the table on the following page.

Table 9. Days with testing and corresponding labelling with A-J.

Week	Day	
1	A	Monday 29 September 2014
	B	Tuesday 30 September 2014
	C	Wednesday 1 October 2014
	D	Thursday 2 October 2014
	E	Friday 3 October 2014
2	F	Monday 6 October 2014
	G	Tuesday 7 October 2014
	H	Wednesday 8 October 2014
	I	Thursday 9 October 2014
	J	Friday 10 October 2014

Week no	Day of week	Test	Description	Notes
1	Monday	A1	Dry test. Friction. Only PTO logging.	
	Tuesday	B01	Step test motor velocity, in water, no waves. Logging on all systems. Wavelab stopped logging after 1000 s.	Water depth, h = 0.600 m ("default")
		B02	Motor acceleration. In water. Full power start on motor and full brake. Logging on all systems.	Webcam not working.
	Wednesday	C01	Hydrostatics. Manual dragging with rope in horisontal direction, first -x (towards generator), afterwards in + x (towards beach)	Force sensor SG reaches limit. Awasys trigger send twice (second one is on WEB-cam)
		C02	Drop test. Manual lift up and release, and later manual push down and release.	Some drift in horizontal direction (but not problematic)
		C03	Freefloat. Regular wave, H_input = 0.05 m, T = 2 s. PTO turned off.	
	Thursday	D01	Fixed float (initial test with first version on fixation). No waves. Step motor velocity in water. (h = 0.653 m)	Water level increased to 65.3 cm (+5.3 cm) as the rigid connection was slightly mis-alligned (float was laying higher in the water). No OptiTrack-data.
		D02	Motor step up in calm water at increased water level (h = 0.653 m).	This test only exist on high water with inclined float (i.e. no motor test was done at normal water level and normal inclination)
		D03	Fixed float (second version on fixation), normal water level. Regular wave RB-series (small waves).	
		D04	Controlled float in regular waves. Machine is started before the waves. Order of execution: RA1, RA3	OptiTrack from last test (RA3) is not available
	Friday	E01	Controlled float in regular waves. Waves are started before the machine, in end waves are stopped and the machine is contioued running for some time before it is braked down (by friction). Order of execution: RA1	Optitrack system updated with an extra ball and camera coordinate system changed.
2	Monday	F01	Dry test. Friction. Only PTO logging.	New rubber-rollers mounted (=> lower friction)
		F02	Calm water test. Two tests, "F02_0position" (a) and "F02_Drop" (b). Drop test where the float is first pulled up and released, afterwards pushed down and released	Pull up test was perfect (see video)
		F03	Controlled float in regular waves. Waves are started before the machine. Order of execution: RA3	
		F04	Controlled float in irregular waves. Waves are started before the machine. Order of execution: IR1	Only Wavelab-data and video. No Optitrack and PTO data can be found.
	Tuesday	G01	Controlled float in regular waves. RA3	Tracking of position out of order in G01. Damaged mounting plate by load sensor. The "30 degree inclined bearing, 8 degree limited" was changed to be "0 degree inclined, unlimited" before the test. Rubber bands was instead used to center the float in the mean position.
		G02	Controlled float in regular waves. RA3 (Repetition of G01), RA2.	
		G03	Step test motor velocity, in water, no waves. Logging on all systems.	Change of mooring lines to more wide and symmetric lay-out. Adding two mooring force sensors to Wavelab data acquisition
		G04	Controlled float in regular waves. Waves are startet before the PTO. Order of execution: RA4	
	Wednesday	H01	Static stiffness test. Manual drag towards beach with line	No PTO-data (not running)
		H02	Horisontal "Release-test". Manual drag towards beach with line (static part), then sudden release (dynamic part)	
		H03	Controlled float in regular waves. RA4	
		H04	Controlled float in regular waves. RA6	
		H05	Controlled float in regular waves. RA5	
		H06	Controlled float in regular waves. RA7	
		H07	Controlled float in irregular waves. PTO is startet before the waves. Order of execution: IR2, IR3	
	Thursday	I01	Controlled float in regular wave (period sweep). I01RC1. PTO speeder setting 3.	
		I02	Controlled float in regular wave (period sweep). I02RC1. PTO constant speed setting control gains : high: 2.9, low: 3.1.	
		I03	Controlled float in regular wave (period sweep). I03RC1. PTO adaptive control.	
		I04	Controlled float in regular wave (negative phase shift). I04RD1. PTO speeder setting 2.95.	
		I05	Controlled float in regular wave (positive phase shift). I05RD1. PTO speeder setting 2.95.	
		I06	Controlled float in regular waves. RA1. Rotated bearing.	Orientation of bearing changed. Arm in wave direction with the float closest to the beach (bearing towards the generator). No video and no Optical tracking data, only WaveLab + PTO data were recorded.
	Friday	J01	Wave tests. No float in water. Regular waves. Order: RD1, RD2, RC1, RAX (in order), RBX (in order)	Recordings with WaveLab and Web-camera only (no PTO and no OptiTrack).
		J02	Wave tests. No float in water. Irregular waves. Order: IR2, IR3	Awasys file for IR1 was overwritten, so this wave could not be generated (i.e waves in basin without float for test F04 could not be generated)

9 Mooring restoring stiffness

During the experiments measurements were performed to estimate the mooring line stiffness. Results are shown below from test H01. The signal is divided into two parts, the first part (blue lines) with a relatively small displacement, and a second part (red lines) with a somewhat larger displacement. From the results some hysteresis it is seen in the mooring lines, and therefore the fit of the mooring stiffness is performed on the data from the small deformation (the blue part).

The mooring stiffness is found by the linear fit to be 149 Nm/rad.

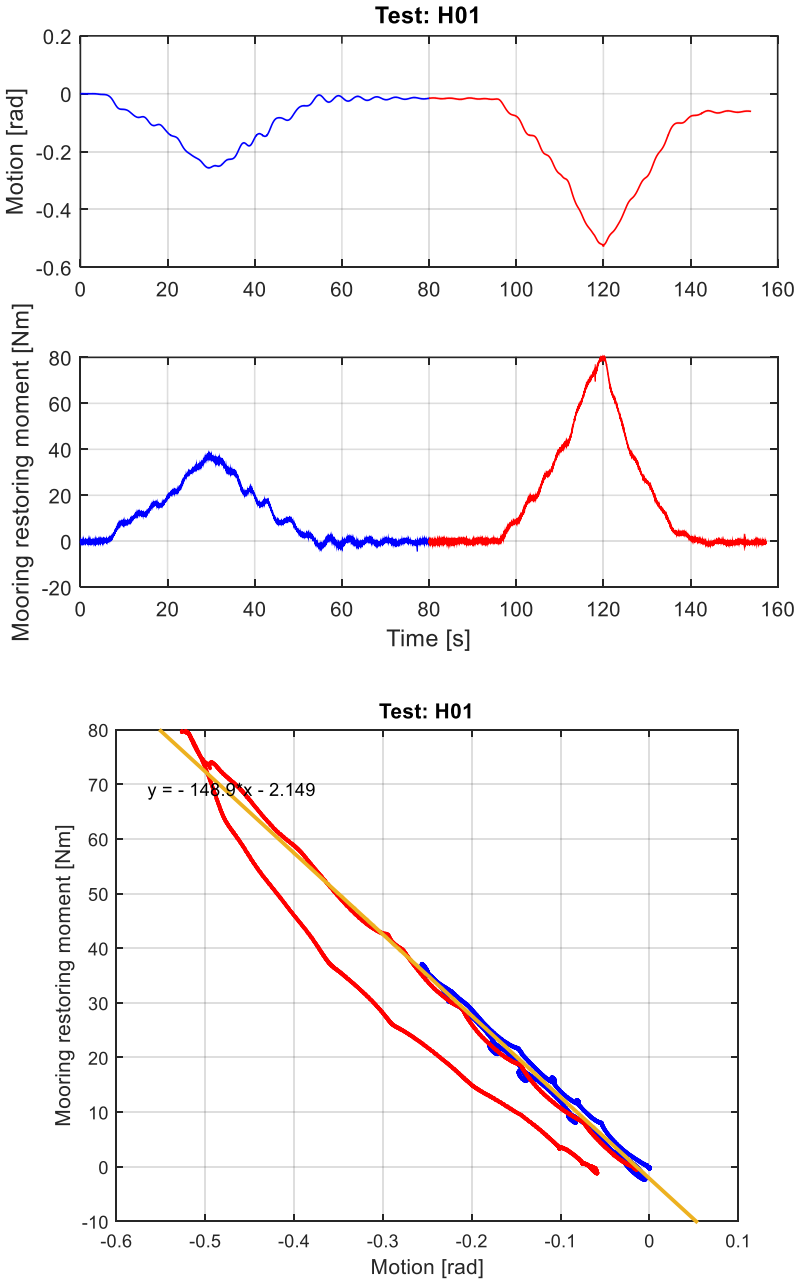

Figure 21. Results of mooring tests. Mooring stiffness = 149 Nm/rad for the yaw DoF.

10 Eigen periods

In order to measure the eigen periods the device was manually moved away from the mean position, then suddenly released, and the response during the following decay was then measured. The raw measurements are shown in Figure 22 where some peaks are marked showing the time and value of the peaks. From the markings it is clear that the eigen period for the vertical motion (roll) was 1.0 s, and the eigen period for horizontal motion (yaw) was 5.0 s, see summary in Table 10.

Table 10. Measured eigen periods for the two external degrees of freedom.

Degree of freedom	Measured eigen period (s)
Roll, φ Rotation about the horizontal x-axis (wave propagation direction) caused by the vertical motion of the ball	1.0
Yaw, θ Rotation about the vertical z-axis caused by the horizontal motion of the ball	5.0

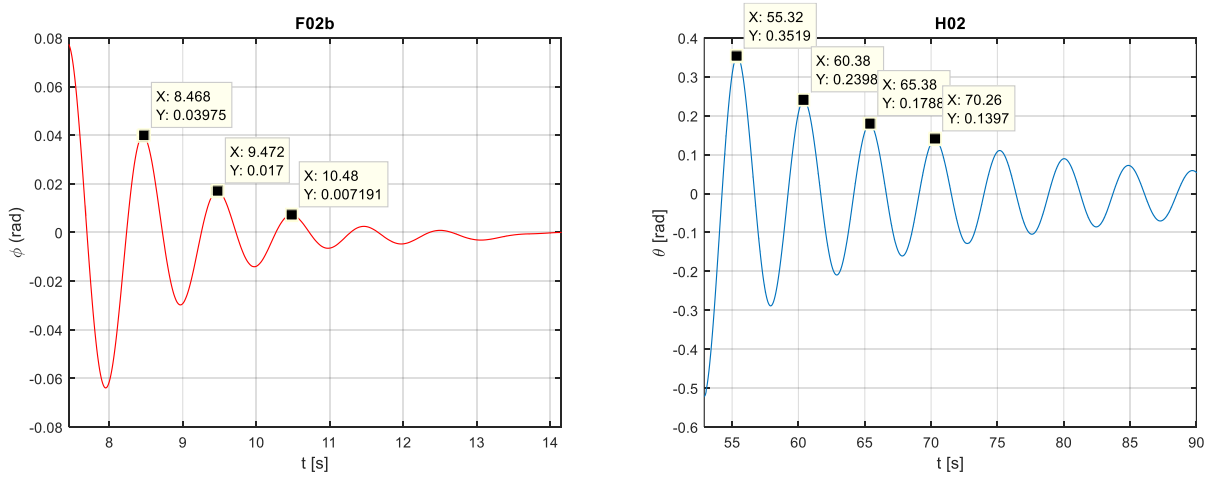

Figure 22. Results of decay tests for the two external degrees of freedom.

11 Friction measurements and power absorption calculation

On Monday the 2nd week the friction was reduced significantly by installing new robber rollers. Therefore two curves have been used to model the friction, see Figure 23.

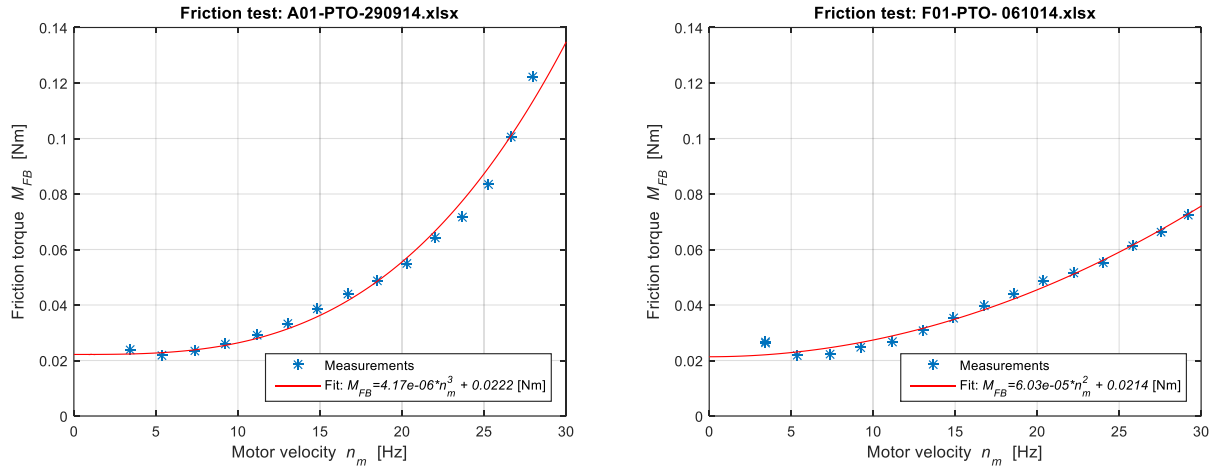

Figure 23. Results of friction tests. Fittet curves are used to find the mechanical work torque.

The friction torque was calculated from the measured motor current and voltage using the code below.

```
% Constants:
Re = 0;              % Electrical resistance (estimated) [ohm]
Rm = 0.363;          % Motor resistance (catalog value) [ohm]
I0 = 0.539;          % No load current (catalog value) [A]
km = 0.0705;         % Torque constant (catalog value) [Nm/A]
MR = km*I0;          % Friction torque [Nm]
Vdc = 1.5;           % Voltage drop over controller (manual value) [V]
Idc = 0.0425;        % Current drain from controller (measured) [A]
ntm = 18;            % Nummber of tooth on motor pulley
ntfl = 40;           % Nummber of tooth on flyweel pulley
Ngear = ntfl/ntm;    % Gearing ratio from flywheel to motor

% Measured values:
PTO_Data = xlsread([PathInputData XlsFile],'Måle data');

Vms = PTO_Data(:,3);     % Motor Voltage (supply voltage/measured) [V]
Ims = PTO_Data(:,2);     % Motor Current (supply current/measured) [A]
nf = PTO_Data(:,8)/100; % Flyweel freq (100 puls pr. rotation)[Hz]

t_PTO = PTO_Data(:,1)-PTO_Data(1,1);
SS_PTO = PTO_Data(:,4); % Speed setting

% Calculations:
Vm = Vms - Vdc;      % Motor Voltage after controller [V]
Im = Ims - Idc;      % Motor Current after controller [A]
nm = nf*Ngear;       % Motor speed [Hz]

Pem = Vm.*Im;        % Elektrical power uptake motor [W]
PL = Re*Im.^2;       % Power loss in electrical system [W]
PJ = Rm*Im.^2;       % Power loss in motor [W]
PM = Pem - PJ - PL;% Mechanical output power [W]

Mm = PM./(2*pi*nm);% Motor torque [Nm]
Ms = Mm - MR;        % Motor shaft torque [Nm]

M_FB = Ms;           % Friction torque in the internal bearings and rubber [Nm]
```

To calculate the power the first part of the procedure is the same as used for the friction estimation, and the shaft torque is calculated in the same way. The friction torque is calculated from the curve depending

on the velocity of the flywheel. The mechanical work torque is finally calculated by subtracting the friction torque from the motor shaft torque.

The absorbed power [W] is found by multiplying the mechanical work torque [Nm] with the spinning velocity [rad/s].

```
Ms = Mm - MR;       % Motor shaft torque [Nm]

if Case(1)=='A' | Case(1)=='B'  | Case(1)=='C'  | Case(1)=='D'  | Case(1)=='E'
    disp('Friction model 1')
    a = 4.166e-06; b = 0.022186; % FO(x) = a*x^3+b
    M_FB = a*nm.^3 + b; % Friction moment measured in test A01 (for test A-E)
else
    disp('Friction model 2')
    a = 6.0301e-05; b = 0.021358; % FO(x) = a*x^2+b
    M_FB = a*nm.^2 + b; % Friction moment measured in test F01 (for test F-J)
end

M_W = Ms - M_FB;    % Mechanical work torque [Nm]

Ph = -2*pi*nm.*M_W; % Harvested absorbed power [W]
```

In order to validate the power calculation the energy in the flywheel was investigated during a breaking event in dry conditions (the last part of test F01). The reference energy was calculated from the velocity and inertia moment of the flywheel (red curve on Figure 24). The estimated power using the equations was integrated over time to give the energy that was accumulated and later taken out of the flywheel during the breaking (blue curve on Figure 24). As the two curves are in good agreement the calculation procedure is found to be reliable.

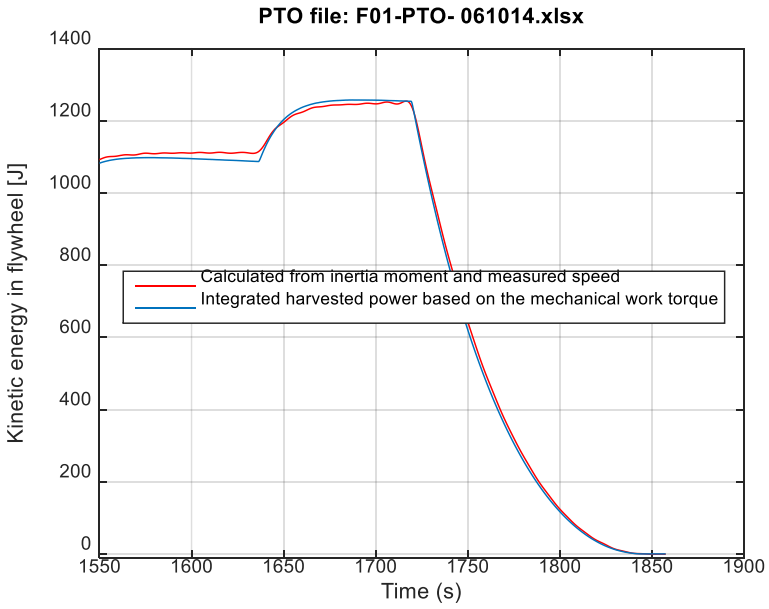

Figure 24. Validation of motor power calculation by looking at energy exchange during breaking event.

12 Wave analysis

The target waves are described in Appendix A. Time series of the actual measured waves are shown in Appendix B, where a selection for the analysis is also given. The actual wave heights in the tables below are taken as the average from the six wave gauges in line with absorber, WG no. 4, 5, 6, 7, 8, 9. All numbers are in agreement with the expectations.

Table 11. Regular wave, "Normal type" (used for PTO tests).

Name	*T* (s)	Target *H* (m)	Actual *H* (m)
RA1	2.00	0.10	0.082
RA2	1.80	0.15	0.138
RA3	2.00	0.15	0.124
RA4	2.20	0.15	0.123
RA5	2.40	0.15	0.150
RA6	2.20	0.20	0.171
RA7	2.40	0.20	0.195

Table 12. Regular wave, "Small type" (used for fixed float tests).

Name	*T* (s)	Target *H* (m)	Actual *H* (m)
RB1	1.50	0.04	0.033
RB2	2.00	0.04	0.034
RB3	2.50	0.04	0.029
RB4	1.50	0.02	0.016
RB5	2.00	0.02	0.017
RB6	1.50	0.01	0.008

Table 13. Regular wave, "Phase shift type".

Name	*T* (s)	Target *H* (m)	Actual *H* (m)
RD1	2.00	0.15	0.111
RD2	2.00	0.15	0.114

Table 14. Regular wave, "Period sweep type"

Name	*T* (s)	Target *H* (m)	Actual *H* (m)
RC1	[1-3]	0.10	0.086

Table 15. Irregular waves

Name	T_P (s)	Target H_{m0} (m)	Actual H_{m0} (m)
IR2	2.6	0.15	0.123
IR3	2.6	0.15	0.124

13 Power performance results based on the motor power

The best performance was achieved during the last three days, Series G, H and I. Focus is therefore on the results from the successful tests during those three days. The analysed tests are given in the tables below. Details are given in the figures on the following pages.

In Table 16 the highest average power output in the regular waves was reaching 13.9 W in test H04RA6, and in this case the capture width was 0.20 m. The shortest wave was giving the highest output, and the capture width was highest for the lowest waves. The highest capture width was found in test G04RA4, where the measured capture width was 0.33 m. The average capture width in the 4 regular tests was 0.21 m.

In Table 17 it is seen that in the period sweep waves the power output was mainly negative, giving negative average output.

In Table 18 with the phase shift wave the device recovered after the negative phase shift of –pi/2 (test I04RD1), and positive production was ensured. However, in the phase shift with a positive phase shift of +pi/2 (test I05RD2) the device did not recover and the power production maintained negative after the phase shift.

As seen in Table 19 the average power production was negative in the irregular waves. Only now and then the power production was positive as seen on the figures subsequently.

Table 16. Regular waves, measured power absorption performance.

Test	Absorbed power (W)	$H_{measured}$ (m)	T (s)	Capture width (m)
G04RA4	11.6	0.123	2.20	0.33
H04RA6	13.9	0.171	2.20	0.20
H05RA5	10.3	0.150	2.40	0.19
H06RA7	10.5	0.195	2.40	0.11

Table 17. Period sweep wave, measured power absorption performance.

Test	Absorbed power (W)	$H_{measured}$ (m)	T (s)
I01RC1	-5.3	0.086	[1-3]
I02RC1	-4.6	0.086	[1-3]
I03RC1	-4.1	0.086	[1-3]

Table 18. Phase shift wave, measured power absorption performance.

Test	Absorbed power (W)	$H_{measured}$ (m)	T (s)	Details
I04RD1	15.5	0.111	2.00	Phase shift of -pi/2 after 4 min.
I05RD2	Unstable	0.114	2.00	Phase shift of +pi/2 after 4 min.

Table 19. Irregular wave, measured power absorption performance.

Test	Absorbed power (W)	$H_{m0,measured}$ (m)	T_P (s)	Details
H07IR2	-2.5	0.123	2.6	Jonswap, gamma = 1
H07IR3	-2.2	0.124	2.6	Jonswap, gamma = 3.3

13.1 Power performance in regular waves

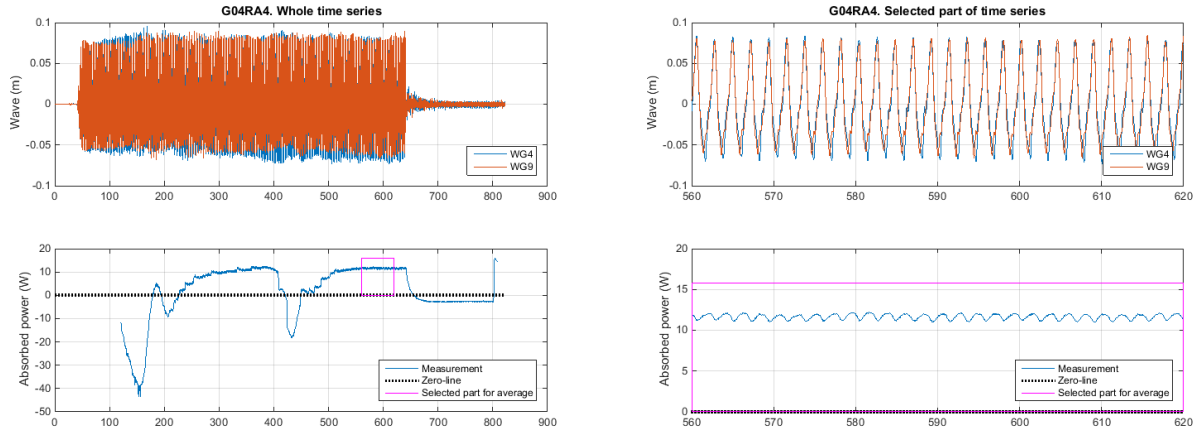

Figure 25. Regular wave test G04RA4.

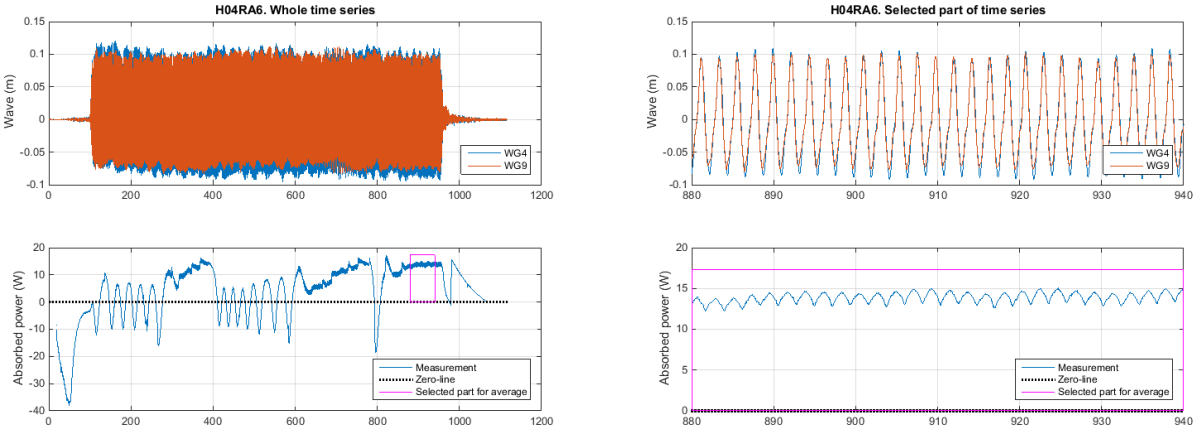

Figure 26. Regular wave test H05RA6.

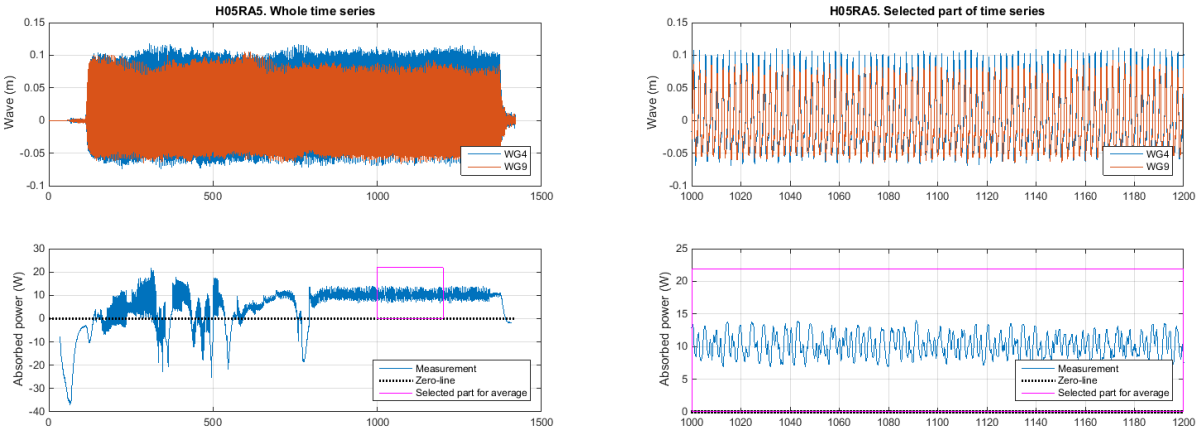

Figure 27. Regular wave test H05RA5.

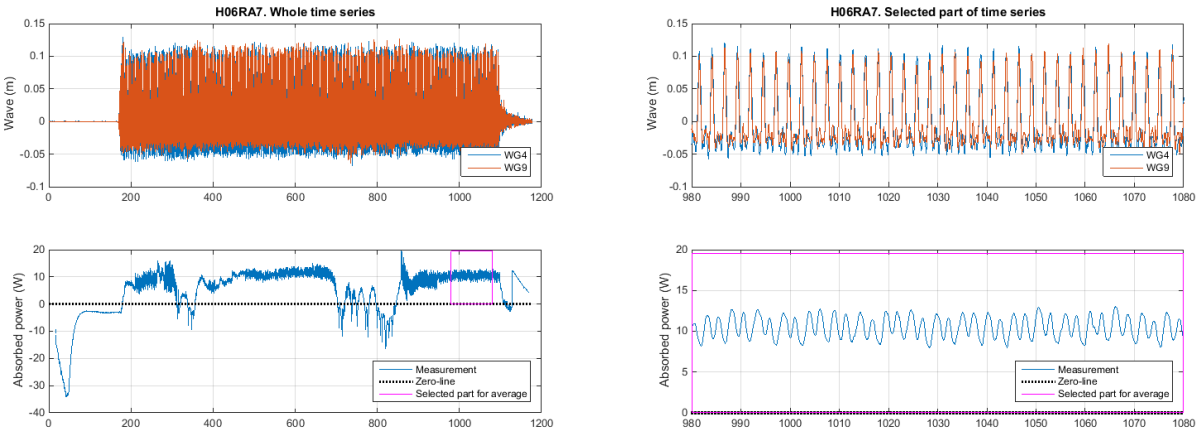

Figure 28. Regular wave test H06RA7.

13.2 Power performance in period sweep wave

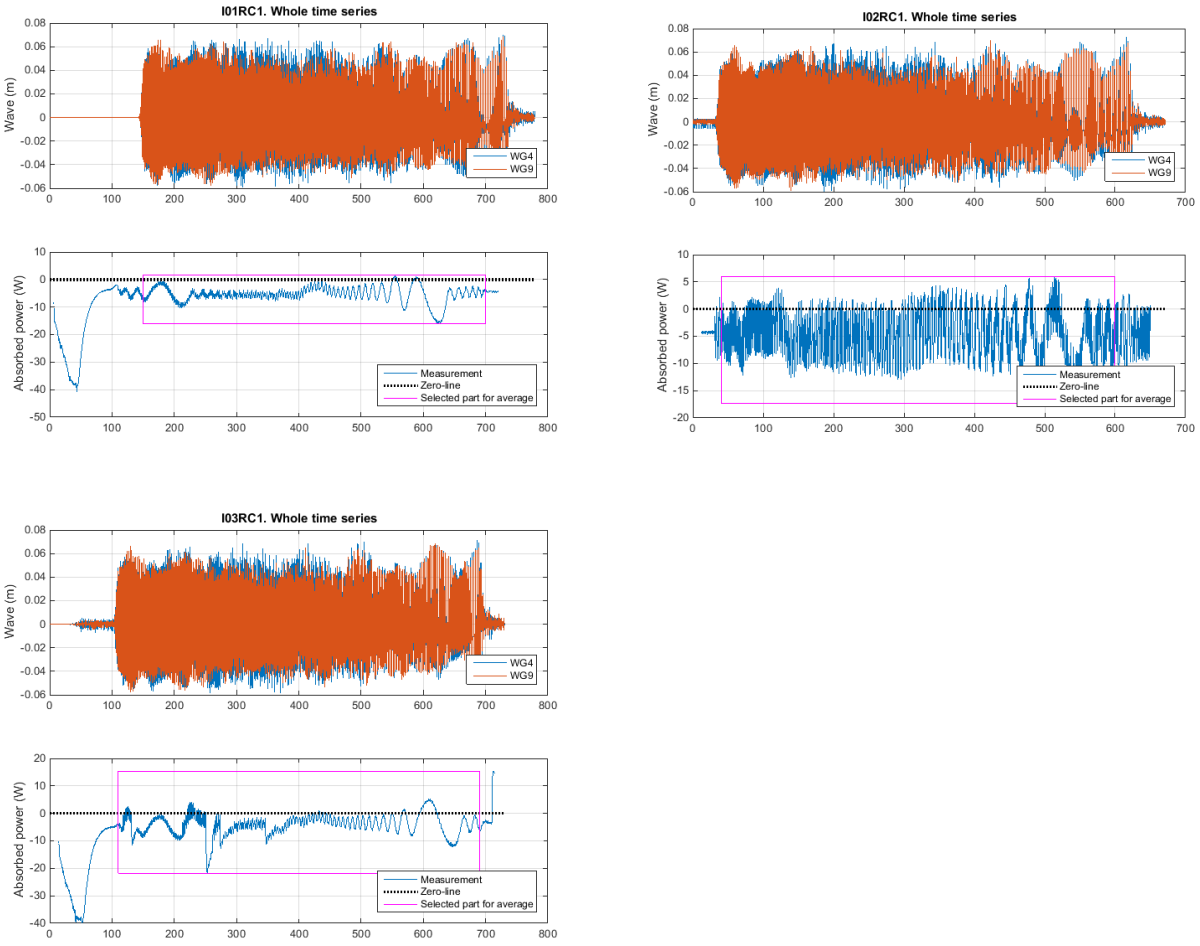

Figure 29. Period sweep test RC1.

13.3 Power performance in phase shift type

In the figure below it is seen that the device recovers after the negative phase shift of –pi/2 (test I04RD1, left graph), and positive production was ensured. However, in the phase shift with a positive phase shift of +pi/2 (test I05RD2, right graph) the device did not recover and the power production maintained negative after the phase shift.

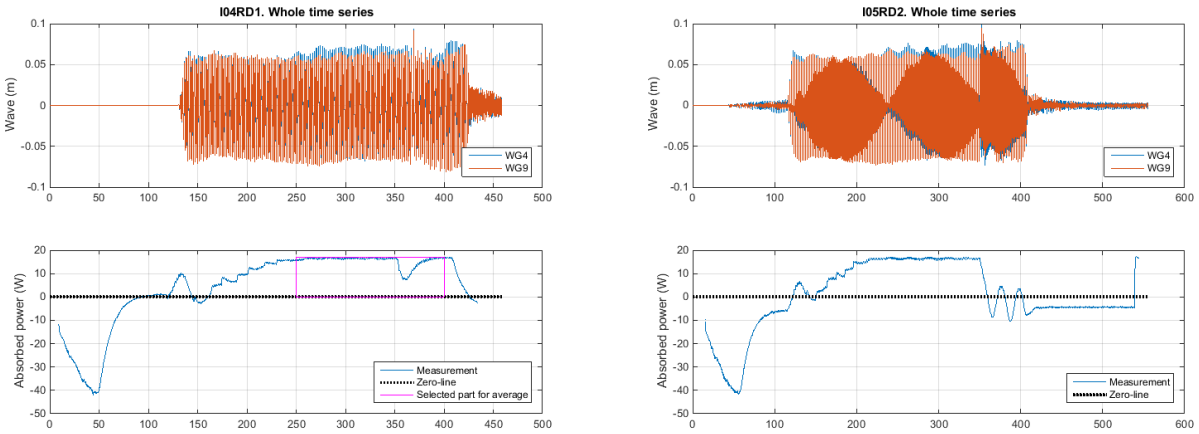

Figure 30. Phase shift wave type.

13.4 Power performance in irregular waves

In the following plots the zoom on the right-hand graph is taken for periods where the power production was positive.

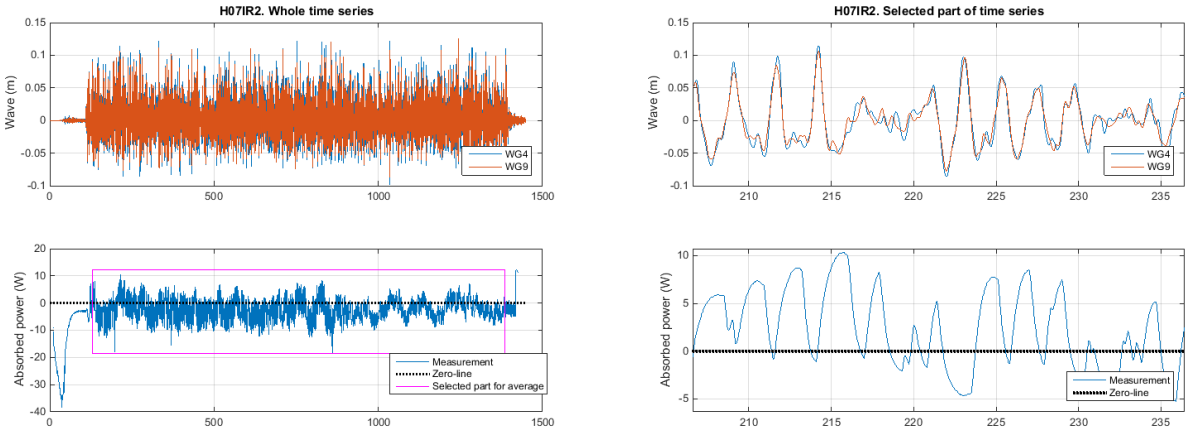

Figure 31. Irregular wave test H07IR2.

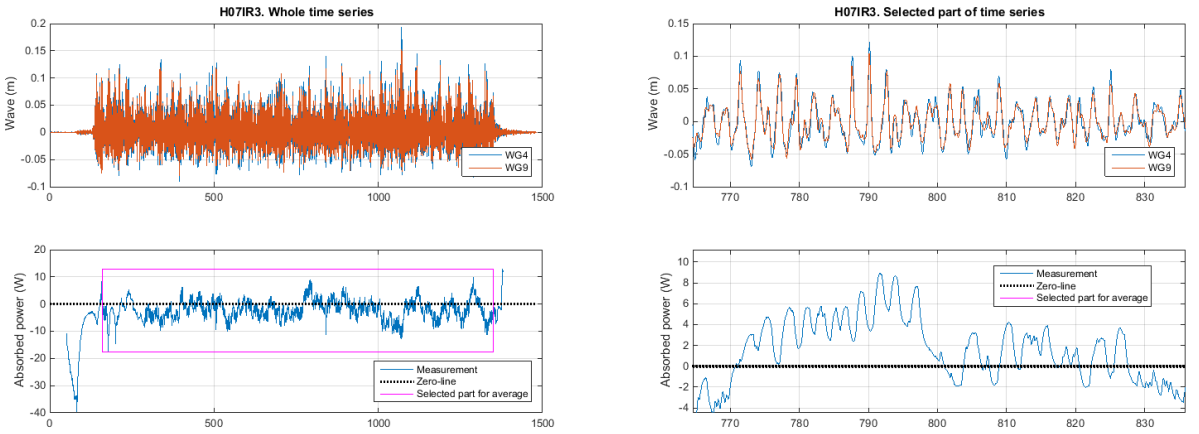

Figure 32. Irregular wave test H07IR3.

14 Alternative power performance estimation based on wave measurements

In the following the power absorption is estimated by using the wave gauge measurements. The wave gauges in front of the device (WG1, 2 and 3) and the wave gauges behind the device (WG10, 11 and 12) are used for the analysis. Two coordinate systems are used, the "G" is located by WG3 on the generator side and system "B" located by WG10 on the beach side, see Figure 33. WG1, 2 and 3 are used to estimate the incoming and reflected wave power at the "G"-system (termed P_{GI} *and* P_{GR} *respectively)*. WG10, 11 and 12 are used to estimate the incoming and reflected wave power at the "B"-system (termed P_{BI} *and* P_{BR} *respectively)*.

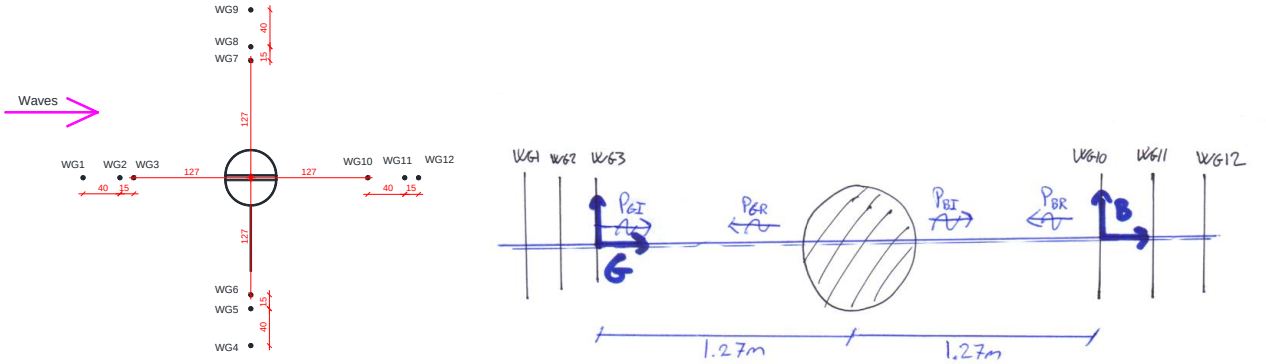

Figure 33. Position of coordinate system "G" (Generator side) and "B" (Beach side). Incident and reflected wave power at the two sides of the floats are shown.

The parameters P_{GI}, P_{GR}, P_{BI} and P_{BR} is the wave power [W/m] given in the coordinate systems. Index:

- G: Generator coordinate system (located by WG3)
- B: Beach coordinate system (located by WG10)
- I: Incoming wave (propagating in positive direction of coordinate system)
- R: Reflected wave (propagating in negative direction of coordinate system)

The absorbed power is estimated by:

$$P_{absorbed} = (P_{GI} - P_{GR} - P_{BI} + P_{BR}) * D * F$$

D is the diameter of the float, *D* = 0.63 m.
F is a factor which takes 3D effects into account. *F* = 4.0 is used.

The factor *F* is estimated in the following by looking at the so-called *Sommerfeld radiation condition*. From this condition it is known that the wave height in a ring wave reduces by one divided by the square root of the distance: $H(r) \sim \frac{1}{\sqrt{r}}$

As the wave power is proportional to the wave height squared, the wave power will decrease by one divided by the distance: $P(r) \sim \left(\frac{1}{\sqrt{r}}\right)^2 = \frac{1}{r}$

By assuming full 2D power P_0 by the distance $D/2$ from the centre of the float, i.e. by the surface of the float, we see that the power by the wave gauge coordinate systems, i.e. in the distance r = 1.27 m, will be reduced to: $P_{WG} = P_0 * \frac{D}{2} * \frac{1}{r} = P_0 * \frac{0.63}{2} * \frac{1}{1.27} = P_0 * 0.248$

The estimation of the factor *F* is thereby found to be: $F = \frac{P_0}{P_{WG}} = \frac{P_0}{P_0 * 0.248} = 4.0$

The wavepower has been calculated using the WaveLab software developed at AAU. Details are given in Excel sheet and a summary is shown in Table 20.

Table 20. Power absorption estimated using the wave gauges.

Test	P_{GI} (W/m)	P_{GR} (W/m)	P_{BI} (W/m)	P_{BR} (W/m)	$P_{absorbed}$ (W)
G04RA4	22.56	1.09	22.31	0.49	-0.87
H04RA6	35.35	2.25	36.67	0.77	-7.06
H05RA5	26.40	0.50	23.78	0.86	7.51
H06RA7	33.81	3.09	31.30	2.88	5.80
H07IR2	11.46	0.80	11.09	0.61	0.44
H07IR3	12.08	0.89	11.53	0.70	0.92
I01RC1	10.16	0.67	10.14	0.43	-0.56
I02RC1	9.96	0.65	9.57	0.40	0.37
I03RC1	9.95	0.66	9.77	0.41	-0.17
I04RD1	26.35	1.11	26.45	1.70	1.25

The incoming wave power on the two sides of the float are almost identical. When trying to extract the small amount of absorbed (positive or negative) power from the relatively large incoming wave power, then the estimated absorbed power is getting very inaccurate.

14.1 Comparison of power based on motor calculations and wave calculations

Table 21. Regular waves, comparison of power calculation methods.

Test	Motor calculations Absorbed power (W)	Wave calculations Absorbed power (W)
G04RA4	11.6	-0.87
H04RA6	13.9	-7.06
H05RA5	10.3	7.51
H06RA7	10.5	5.80

Table 22. Period sweep wave, comparison of power calculation methods.

Test	Motor calculations Absorbed power (W)	Wave calculations Absorbed power (W)
I01RC1	-5.3	-0.56
I02RC1	-4.6	0.37
I03RC1	-4.1	-0.17

Table 23. Phase shift wave, comparison of power calculation methods.

Test	Motor calculations Absorbed power (W)	Wave calculations Absorbed power (W)
I04RD1	15.5	1.25
I05RD2	Unstable	-

Table 24. Irregular wave, comparison of power calculation methods.

Test	Motor calculations Absorbed power (W)	Wave calculations Absorbed power (W)
H07IR2	-2.5	0.44
H07IR3	-2.2	0.92

From the results in Table 21 to Table 24 it is seen that the absorbed power based on the wave measurements does not give reliable results, and the results should not be used to indicate the performance of the device. It is concluded that the power based on the motor power calculations are much more accurate.

15 Alternative power performance estimation based on the reaction forces and motions

The absorbed power by the gyroPTO is calculated following the D'Alembert's principle, using the reaction forces at the base of the system, the mooring forces and the motions of the "absorber". Figure 34 indicates where the reaction forces are measured (at the base of the system through the 6DoF sensor) and where the two mooring forces are.

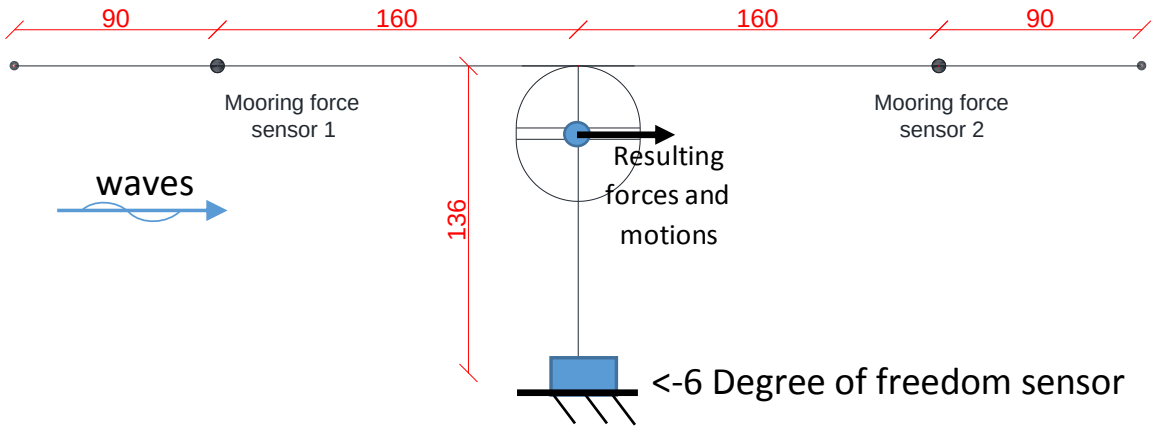

Figure 34. Overview of system.

The absorbed power is a result from the motions of the "absorber" (=the round object) and the forces at its base (6DoF sensor) and the mooring forces. The whole system is assumed to be rigid and all the forces and motions are referred to the centre of the float. The resulting forces at the float is found by adding the mooring forces and the reaction forces from the 6DoF sensor.

To be verified, before making any calculations:

- Signals from different DAQ systems need to be synchronised. This can (easiest) be done by comparing the mooring force signal with the position of the "absorber".
- Force signal or others should off course not be saturated
- Positive axes of forces at base and motions should coincide
    - Fx (6DoF) points downwards
    - Fy (6DoF) points to the wave paddles
    - Fz (6DoF) points to the "absorber"
    - Angle Θ corresponds to horizontal motion of the "absorber", positive to wave paddles.
    - Angle φ corresponds to vertical motion of the "absorber", positive upwards. Note that this signal has to be "turned", in order to match the same coordinate system as the one of the forces. This is then in the opposite direction than the global reference system.
- Resulting mooring force signal (Fm1 – Fm2), needs to be deducted for the horizontal force at its base.
- Vertical motions are small relative to length of the mooring lines, so vertical mooring forces are neglectable.

The velocity of the "absorber" was calculated based on the angles:

$$v_{horizontal\ or\ vertical} = 1.054\ x \frac{\Delta \sin(\phi\ or\ \theta)}{\Delta t}$$

The equation to calculate the power is:

$$P = (F_{horizontal} - (F_{mooring\ 1} - F_{moooring\ 2})) \times v_{horizontal} + F_{horizontal} \times v_{horizontal}$$

15.1 Resulting plots for regular wave test G04RA4

The motions during the whole test:

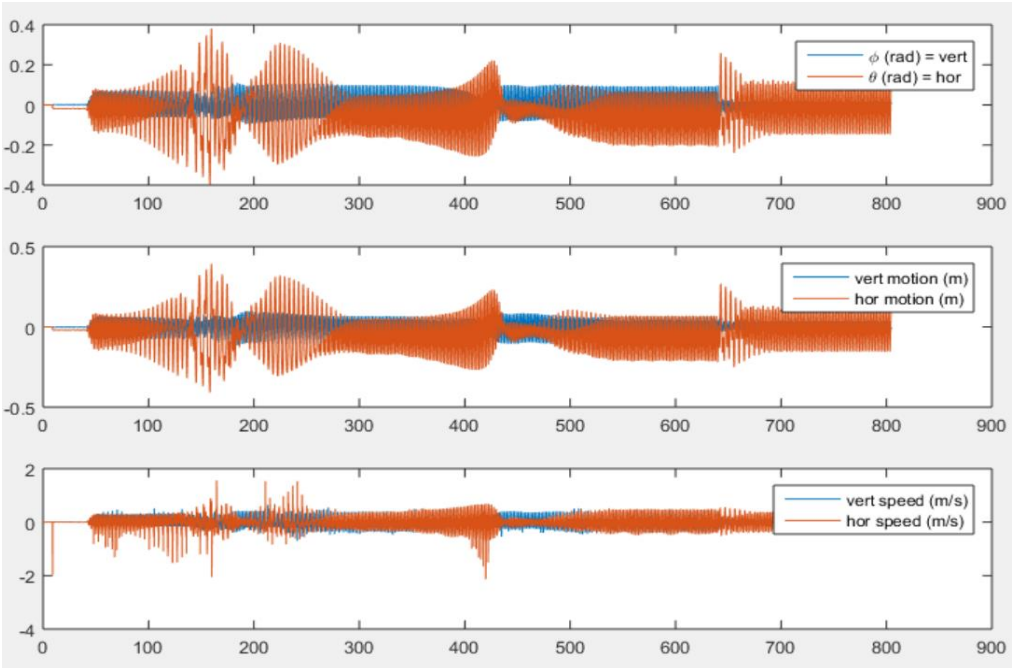

Figure 35 represents the angle at the base (top), the position relative to the rest position (middle) and the velocity of the device (bottom) for the whole test.

The motions during the test are not regular all the time, thereby a stable fraction of this will be selected. The synchronisation is done correctly, based on the beginning of the motions and mooring forces.

The forces during an extract of a stable moment during the test:

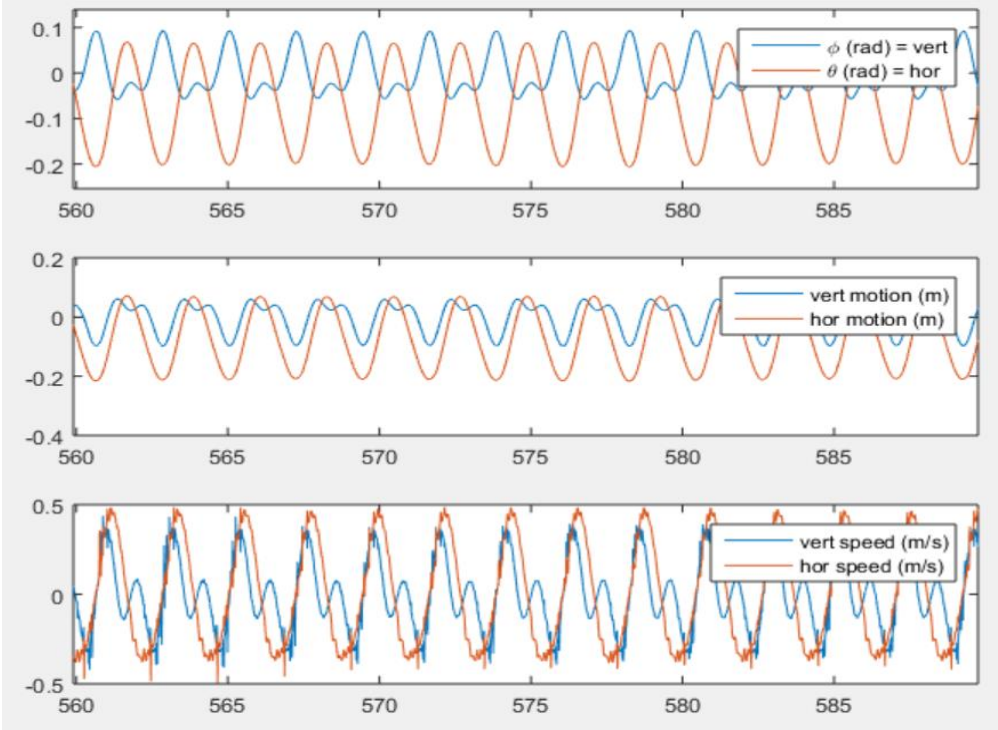

Figure 36 represents the angle at the base (top), the position relative to the rest position (middle) and the velocity of the device (bottom) for a part of the test.

The signals show a very regular pattern.

The forces with the motions:

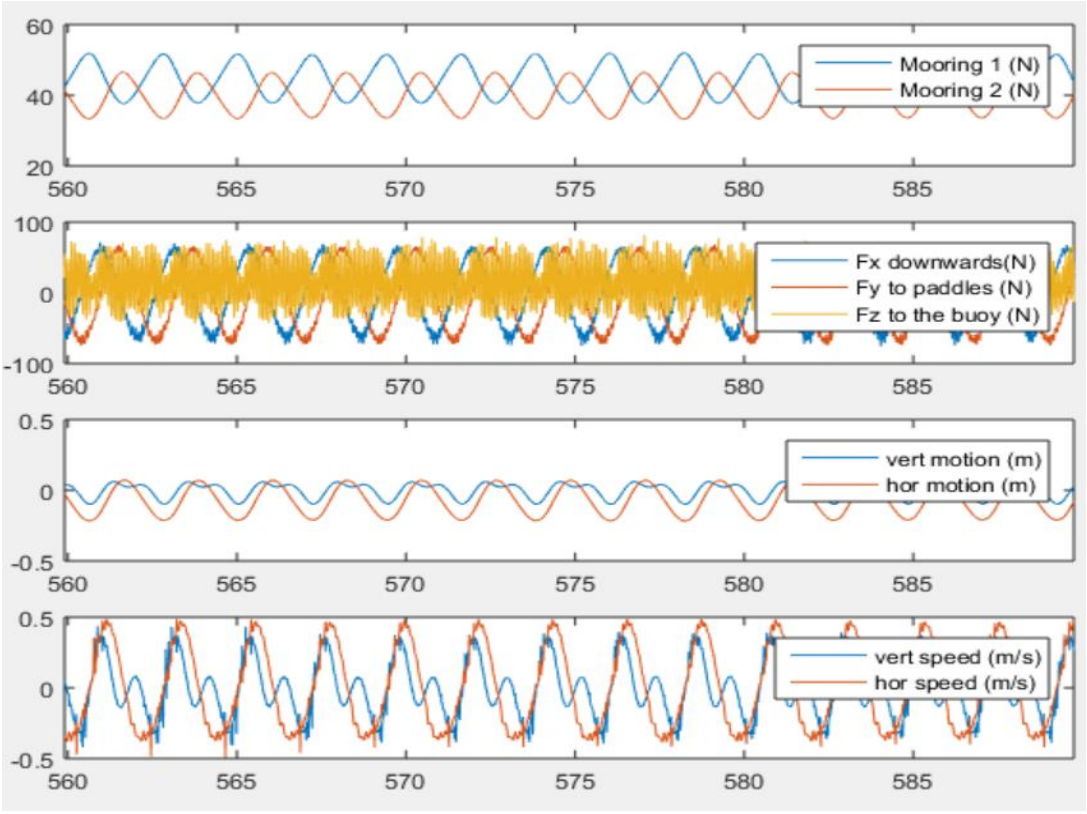

Figure 37 represents the mooring forces (top), the forces at the base (second), the position of the device (third), and the velocity of the device (bottom).

The signals show again a very regular pattern.

Resulting forces and motions:

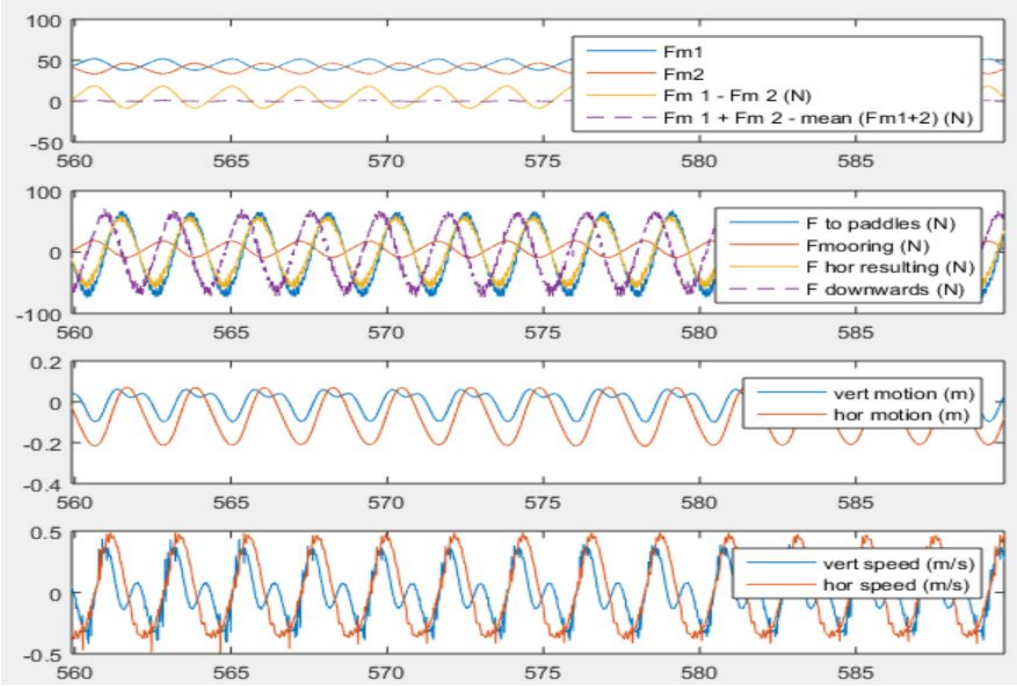

Figure 38 represents the mooring forces (top), the resulting forces on the device (second) , the position of the device (third), and the velocity of the device (bottom).

The signals are again steady.

Force, motions and power:

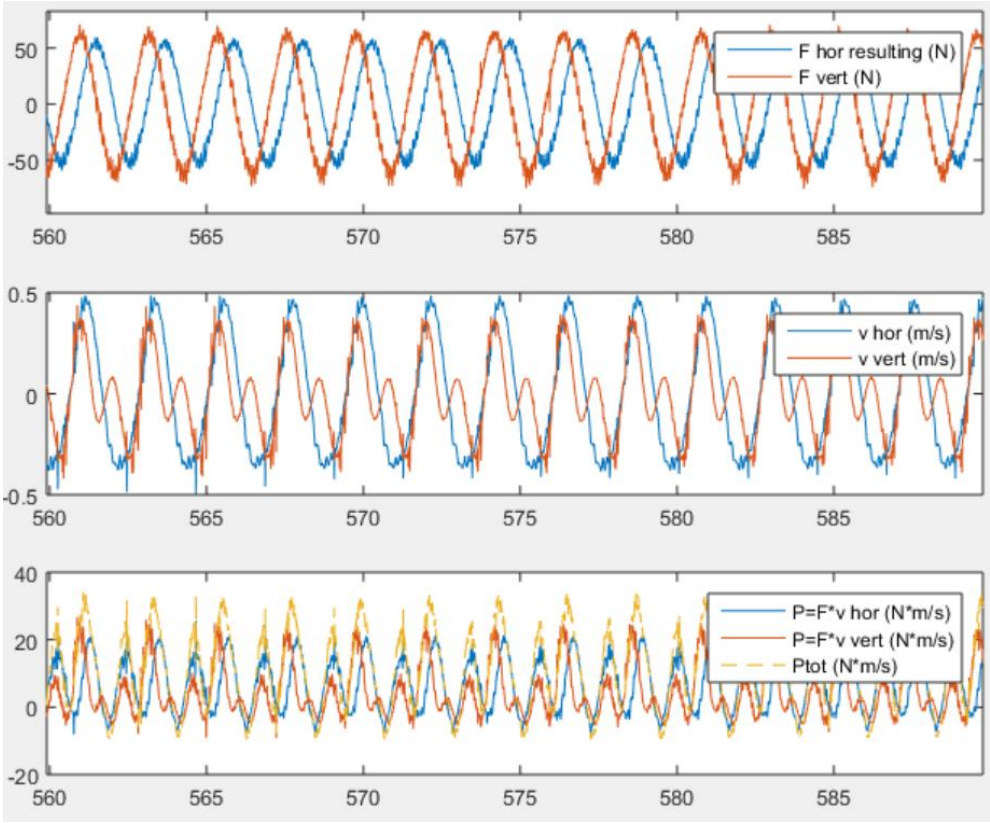

Figure 39 represents the resulting forces on the device (top), the velocity of the device (middle), and the measured power (bottom).

The force and velocity signals are close to be in phase and present a positive power absorption. Compared to the absorbed power curves in the main report, the fluctuations here are much larger and frequent, as they go from approx. zero to 35 W during each period. In the main report the absorbed power is much more constant and close to 12 W (page 29 of main report). This is probably due to the smoothening effect of the flywheel.

In the following figure, the power absorption is presented over the whole file:

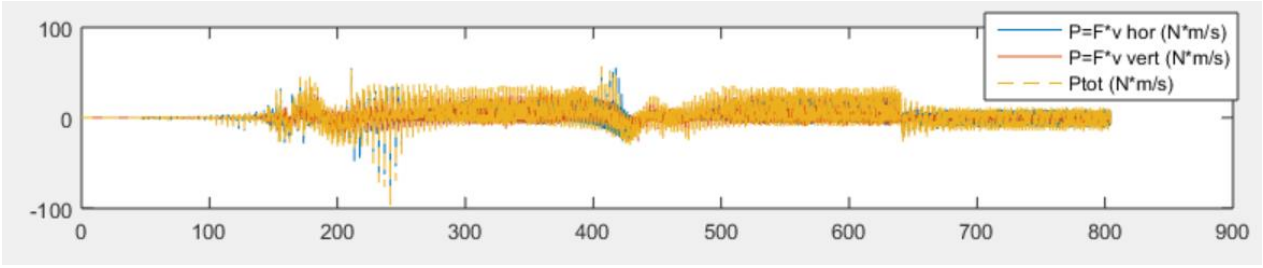

Figure 40 represents the measured power over the whole test.

The power absorption fluctuates over the length of the test, with some stable moments.

For the test period between 200 and 800 s (almost full test), the calculation gives a power absorption of 4.86 W (2.9 W horizontal and 1.96 W vertical).

For the test period between 560 and 620 s (≈ approx. best part of the test), we calculation gives a power absorption of 11.2 W (6.77 W horizontal and 4.4 W vertical).

The power performance results based on the motor power presented an absorbed power of 11.6 W for the test period between 560 and 620s, which is thereby very close but slightly above the value here.

15.2 Resulting plots for irregular wave test H07IR2

The following plots are selected from the signal from test "H07IR2".

The motions for the whole test:

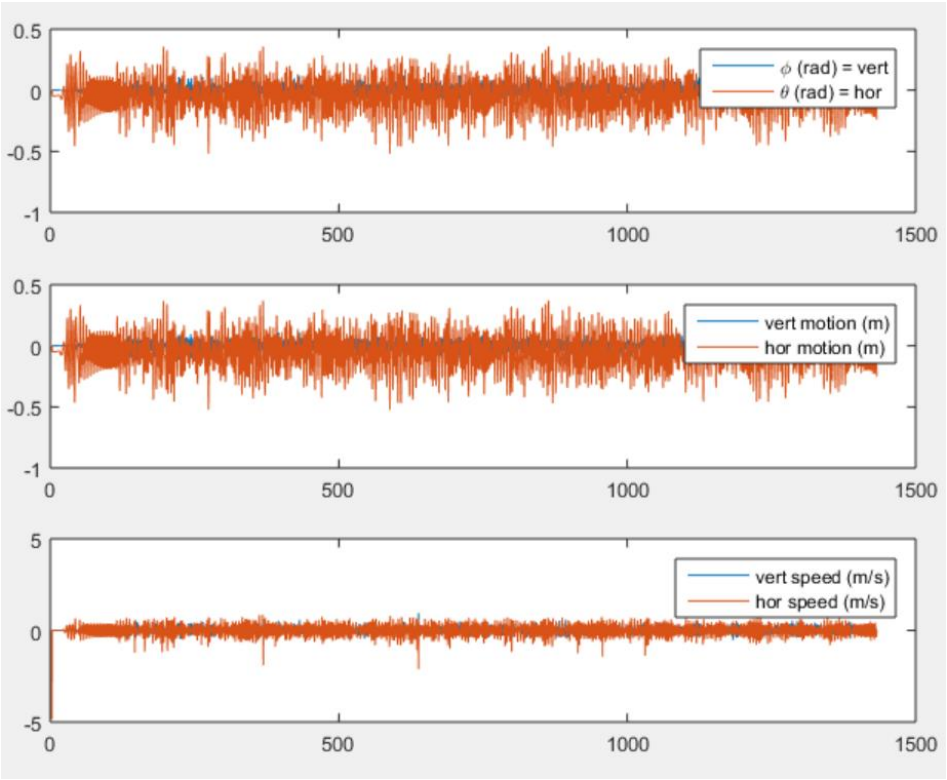

Figure 41 represents the angle at the base (top), the position relative to the rest position (middle) and the velocity of the device (bottom) for the whole test.

The motions for a random part of the test:

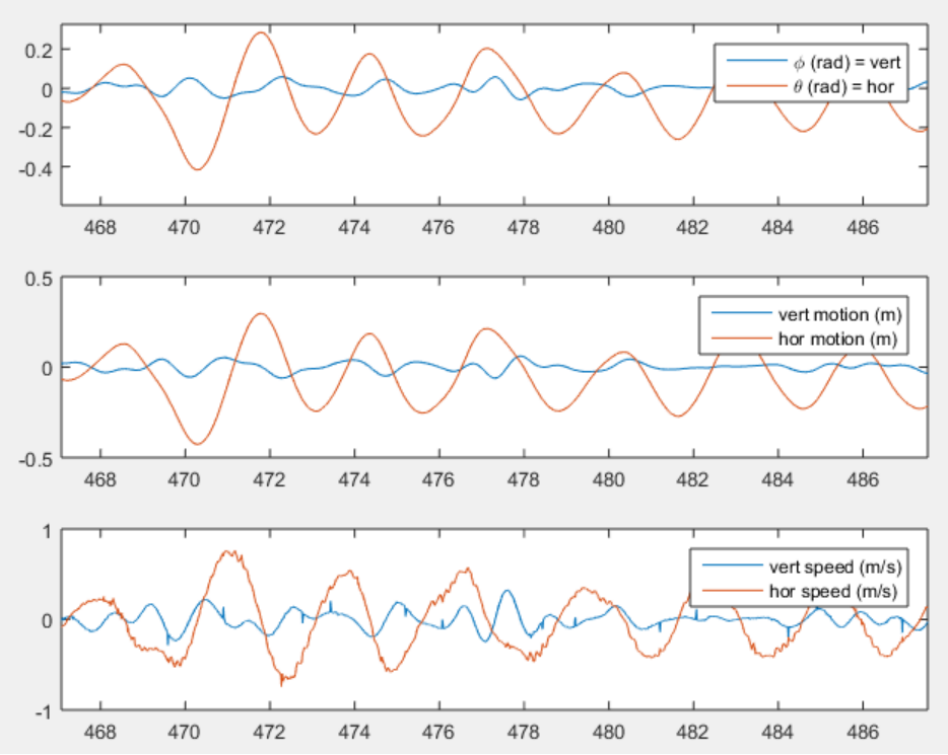

Figure 42 represents the angle at the base (top), the position relative to the rest position (middle) and the velocity of the device (bottom) for a part of the test.

These signals appear to be good.

The forces with the motions:

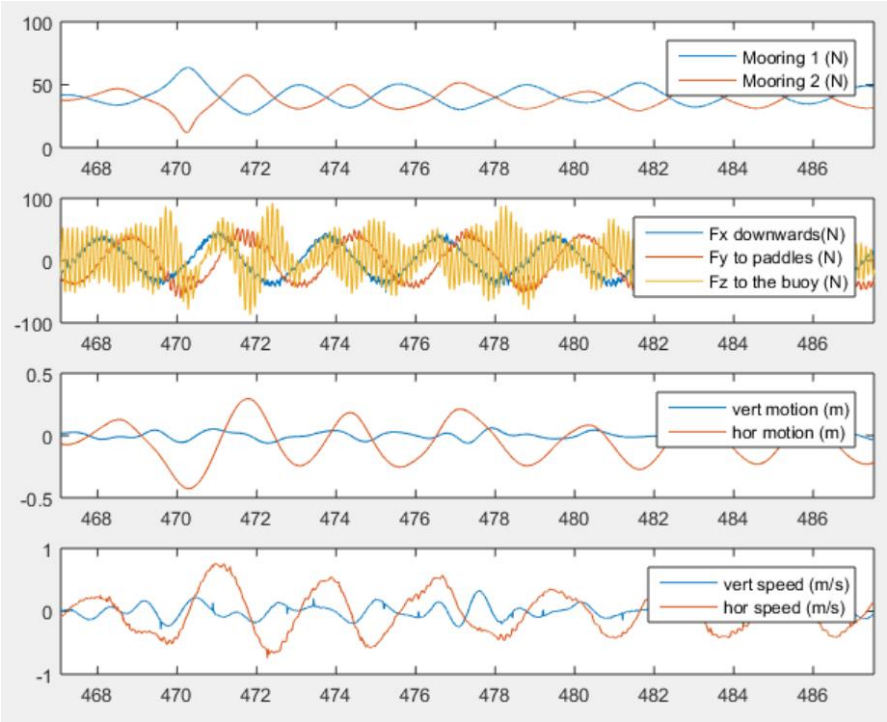

Figure 43 represents the mooring forces (top), the forces at the base (second), the position of the device (third), and the velocity of the device (bottom).

The signals appear to be good, however there is a significant high frequency force on the base 6DoF sensor in the direction of the "absorber".

Resulting forces and motions:

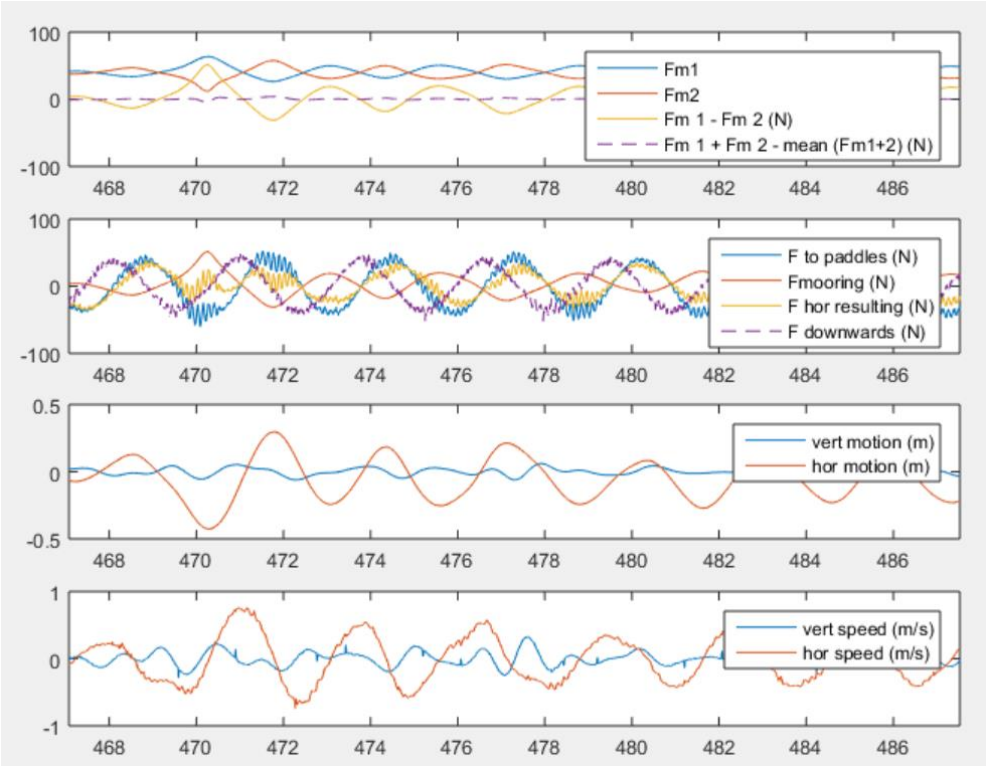

Figure 44 represents the mooring forces (top), the resulting forces on the device (second), the position of the device (third), and the velocity of the device (bottom).

The mooring forces can easily be deducted from each other. The sum of them minus their average gives a very small force, indicating that the vertical forces from the mooring lines are neglectable. The mooring forces seem to be deducted correctly from the horizontal force at the base (second figure).

Force, motions and power:

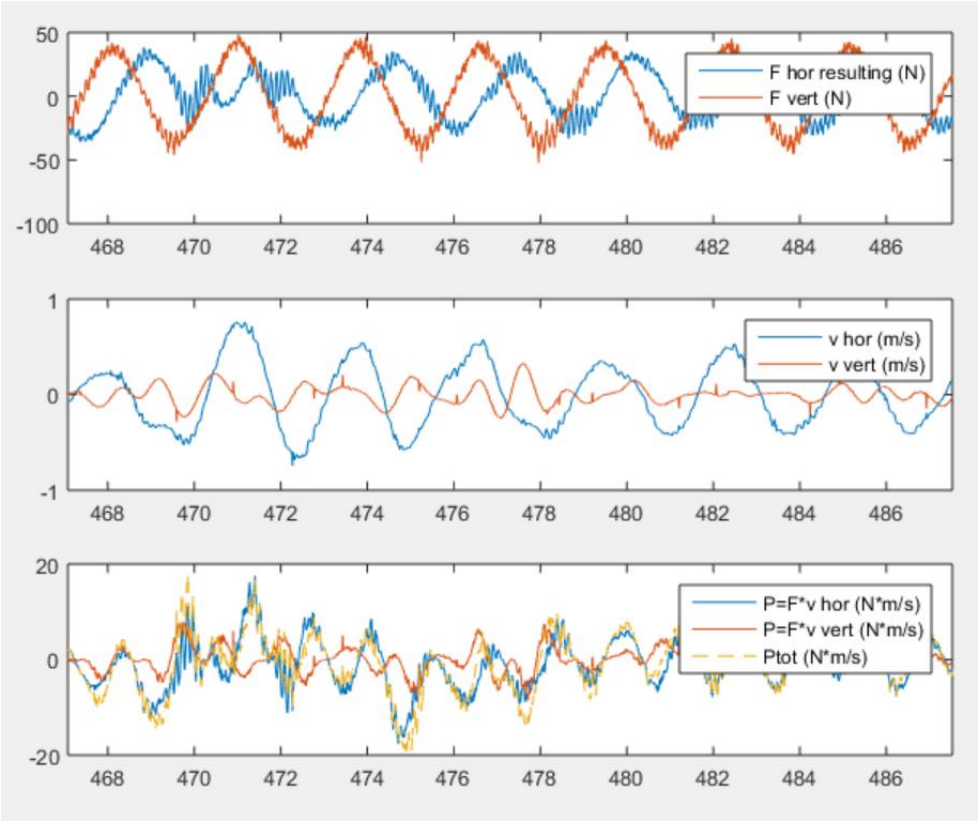

Figure 45 represents the resulting forces on the device (top), the velocity of the device (middle), and the measured power (bottom).

The absorbed power curves over the whole test:

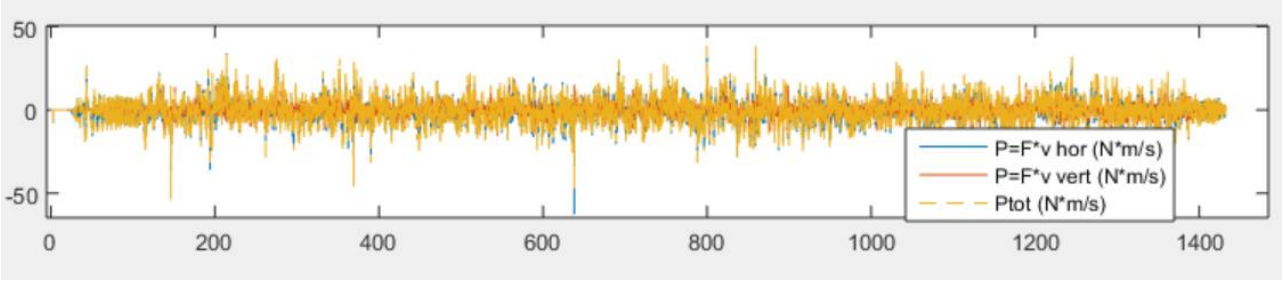

Figure 46 represents the measured power over the whole test.

The horizontal and vertical forces at the base are very regular. The motions are not as regular, in the horizontal motions a pattern can be found, however this is not appearing on the vertical motions. The overall absorbed power fluctuates around zero at a frequency twice larger than the forces at the base, and the horizontal power is thereby in general greater than the vertical power.

In the following figure, the power absorption over the same time frame as with the motor power is represented (which can be visualised on page 31).

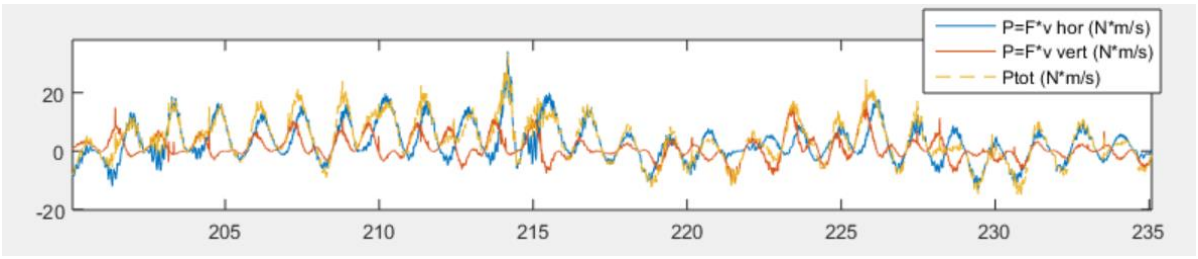

Figure 47 represents the measured power over a part of the test.

As for the regular waves, the absorbed power fluctuates much more in this case. The period of fluctuations are shorter and the amplitudes higher. This must be due to the smoothening effect of the flywheel.

This calculation result in an overall absorbed power of -0.35 W (-0.25 W horizontal and -0.10 W vertical) for the test period between 200 and 1300s, meaning that the system injected more power in the waves, than it absorbed from it. This is slightly different from what was obtained based on the motor power (-2.5 W), however, the calculation based on the motor power is believed to be by far the most accurate. The assumption of having a stiff system is not valid any longer during these conditions.

15.3 Comparison of power based on motor calculations and force-motion calculations

This calculation method (based on reaction forces and motions) gives results of power absorption in the same order of magnitude than with the calculation method based on the motor results. This means that the GyroPTO presents positive power absorption values in regular waves, but negative ones in irregular waves, see Table 25 and Table 26.

Table 25. Regular waves, comparison of power calculation methods.

Test	Motor calculations Absorbed power (W)	Force-motion calculations Absorbed power (W)
G04RA4	11.6	11.2

Table 26. Irregular wave, comparison of power calculation methods.

Test	Motor calculations Absorbed power (W)	Force-motion calculations Absorbed power (W)
H07IR2	-2.5	-0.35

Another observation is that the absorbed power through this method results in much more fluctuating curves, compared to the method in the main report. This results from the power smoothening effect of the flywheel, which is not having an effect on this method of calculation.

The power estimation based on the motor power is believed to be by far the most accurate, as it represents a more direct measurement of the power with less assumptions.

16 Conclusions

The device was initially tested in regular waves with different wave periods and amplitudes. The testing demonstrated that with properly tuned control gains it was possible to achieve a positive power output as long as the waves were constant and sinusoidal. However, it turned out during the testing that the device was extremely sensitive to changes in the wave shape. Therefore two special waves were generated, one type where the phase was slightly altered at a certain instant in time, and one type where the wave period was slowly changed over time. The device was further tested in irregular waves which in larger scale corresponds to the conditions in Nissum Bredning and the North Sea. In the special waves and the irregular waves the performance was generally very unstable, and the measured power absorption was negative most of the time.

The main conclusion on the testing is that more focus should be put into ensuring a stable and positive power output in a variety of wave conditions. It is recommended to look into if more advanced control schemes possibly in combination with physical changes can ensure the stability of the device in irregular waves. The hydrodynamic coefficients in Appendix C can be used for numerical simulations, as described in the paper by Nielsen et al (2015).

The power absorption has in addition been estimated in two other alternative ways, which are represented in chapters 14 and 15. The power production estimation based on the wave measurements appeared to be very inaccurate, however the results with the method based on the reaction forces and motions of the absorbed absorption were in the same order of magnitude than the ones from the power results. In any case, the power performance estimation based on the motor results are the most reliable as they are the most direct and were based on the least assumptions.

17 A rough estimate of the production at larger scale

In the irregular waves the power production was negative and therefore it does not make sense to scale up the results directly. Let us instead suppose for the sake of argument that the power production in irregular waves can somehow be made stable, and further that a continuous production as high as in the regular waves can be achieved. The average measured capture width in the regular waves was 0.21 m. As the device width is 0.63 m this corresponds to a capture width ratio of: 0.21/0.63 * 100 = 33 %. Let's assume that it is possible to get the device to produce as well in irregular waves under any wave conditions, and lets further assume that the yearly absorbed energy can be converted into electricity at a PTO-efficiency of 90 %. Under all those assumptions the results in Table 28 are found, i.e. a Nissum Bredning would produce 0.87 MWh/year and a North Sea device 85 MWh/year.

It should be underlined that the assumptions are presumably unrealistic, and the results can be seen as an idealised maximum of what can be expected. To get reliable estimates the stability of the device should be ensured in irregular waves, and testing should afterwards demonstrate that positive power production can be achieved in a variety of irregular wave conditions.

Table 27. Scale relative to the lab device of the Nissum Bredning device and a hypothetical North Sea device.

Parameter	Laboratory model	Nissum Breding	North Sea
Float size (m)	0.630*0.550	Ø 1.5	Ø 5
Float volume (m^3)	0.104	1.77	65.4
Scale relative to lab	1	2.57	8.57
Power rating	90 W	5 kW	250 kW

*Table 28. Rough estimate of possible production at larger scale. Based on performance measure in **regular** waves.*

Parameter	Nissum Breding	North Sea
Wave power (kW/m)	0.22	6.5
Wave power in device width (kW)	0.33	32.5
Absorbed power if CWR = 33 % (kW)	0.11	10.8
Absorbed yearly energy (MWh/year)	0.96	95
Electrical energy if PTO efficiency is 90 % (MWh/year)	0.87	85

18 References

Johannes Falnes (2005). *Ocean Waves and Oscillating Systems*. Published by Cambridge University Press. ISBN: 9780521017497

O. M. Faltinsen (1993). *Sea Loads on Ships and Offshore Structures*. Published by Cambridge University Press. ISBN: 0521458706

SRK. Nielsen et al. (2015). *Stability analysis of the GyroPTO wave energy point absorber*. Journal paper in preparation.

WAMIT. *WAMIT User Manual*. Download at http://wamit.com/manual.htm

Appendix A: Target wave details

Target parameters are given in the tables below.

Regular waves

Table 29. Target wave conditions in regular waves

"Normal type" (used for PTO tests)					
Name	**H (m)**	**T (s)**		**L0 (m)**	**s0 = H/L0**
RA1	0.10	2.00		6.24	0.0160
RA2	0.15	1.80		5.05	0.0297
RA3	0.15	2.00		6.24	0.0240
RA4	0.15	2.20		7.55	0.0199
RA5	0.15	2.40		8.99	0.0167
RA6	0.20	2.20		7.55	0.0265
RA7	0.20	2.40		8.99	0.0223

"Small type" (used for fixed float tests)					
Name	**H (m)**	**T (s)**		**L0 (m)**	**s0 = H/L0**
RB1	0.04	1.50		3.51	0.0114
RB2	0.04	2.00		6.24	0.0064
RB3	0.04	2.50		9.75	0.0041
RB4	0.02	1.50		3.51	0.0057
RB5	0.02	2.00		6.24	0.0032
RB6	0.01	1.50		3.51	0.0028

"Period sweep type"				
Name	**H (m)**	**T (s)**	**Length**	**Comments**
RC1	0.10	[1-3]	10 min	Linear frequency sweep from T = 1 s to T = 3 s

"Phase shift type"			
Name	**H (m)**	**T (s)**	**Length**
RD1	0.15	2.00	5 min. Phase shift of -pi/2 after 4 min.
RD2	0.15	2.00	5 min. Phase shift of +pi/2 after 4 min.

Irregular waves

Table 30. Target wave conditions in irregular waves

Name	**H_{m0} (m)**	**T_P (s)**	**Length**	**Details**
IR2	0.15	2.6	30 min	gamma = 1, Jonswap (PM-Spectrum) with white
IR3	0.15	2.6	30 min	gamma = 3.3, Jonswap with white noise

Details about the period sweep type

The signal is generated to have a total length of 65536 datapoints. Sampling frequency = (65536-1)/(10*60) = 109.225 Hz. Matlab script used for the generation: "Wave_PeriodChange.m". The matlab function "chirp" is used to generate the sweep: S = a*chirp(t,1/Tmin,t(end),1/Tmax);

Sweep is performed using a linear change in frequency. Full length of 10 minutes is shown on the first figure below, followed by zooms on the first and last part.

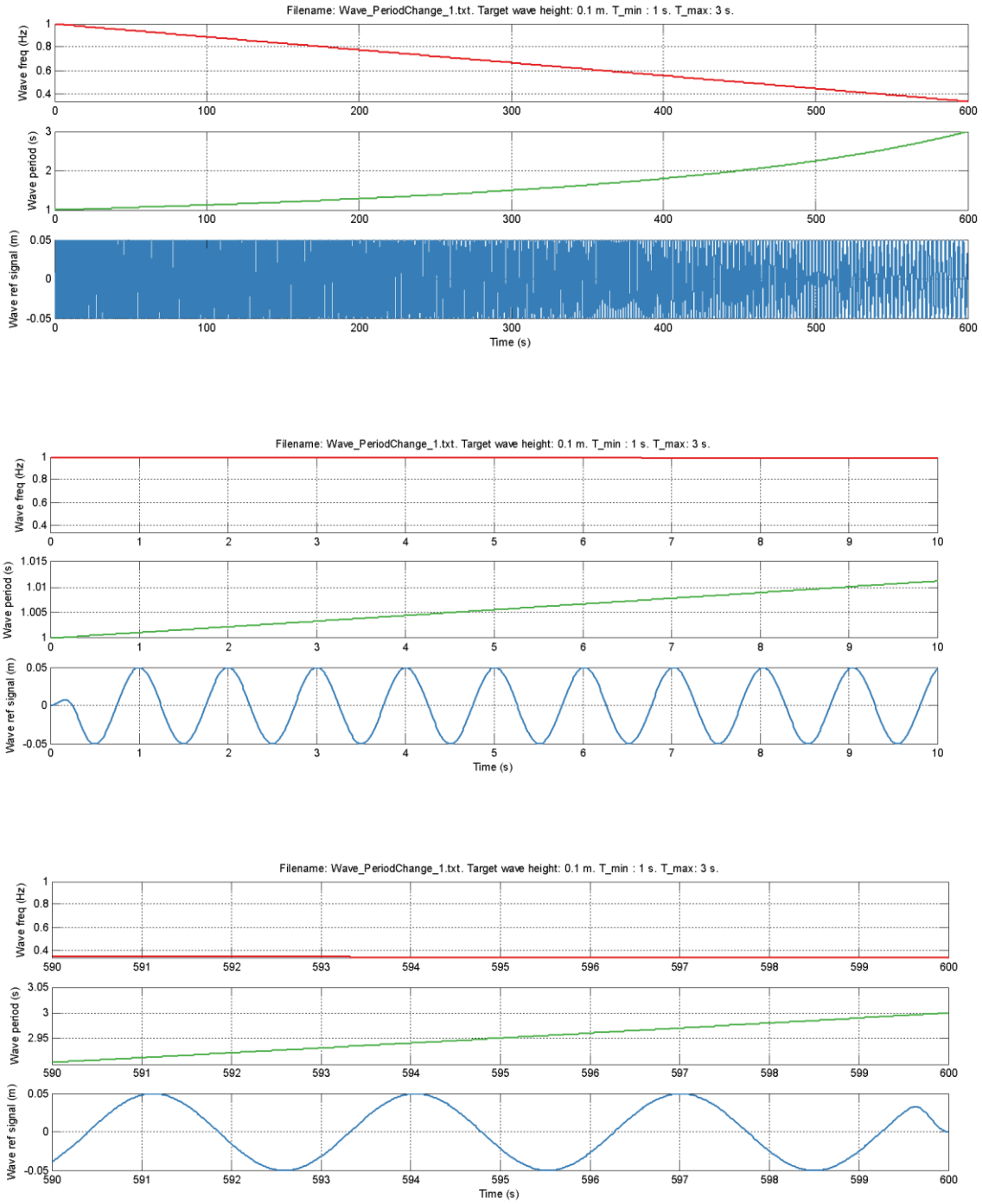

Figure 48 represents the period sweep type.

Details about the phase shift type

The signal is generated to have a total length of 65536 datapoints. Sampling frequency = (65536-1)/(5*60) = 218.45 Hz. Matlab script used for the generation: "Wave_PhaseChangeVer2.m". Wave signal is given by: S = a*cos(2*pi/T*t+d), where d is the phase.

Phase shift is performed linearly and finished within a period of T/2, see plots below. Full length of 5 minutes is given on the first figure, followed by a zoom by the phase shift.

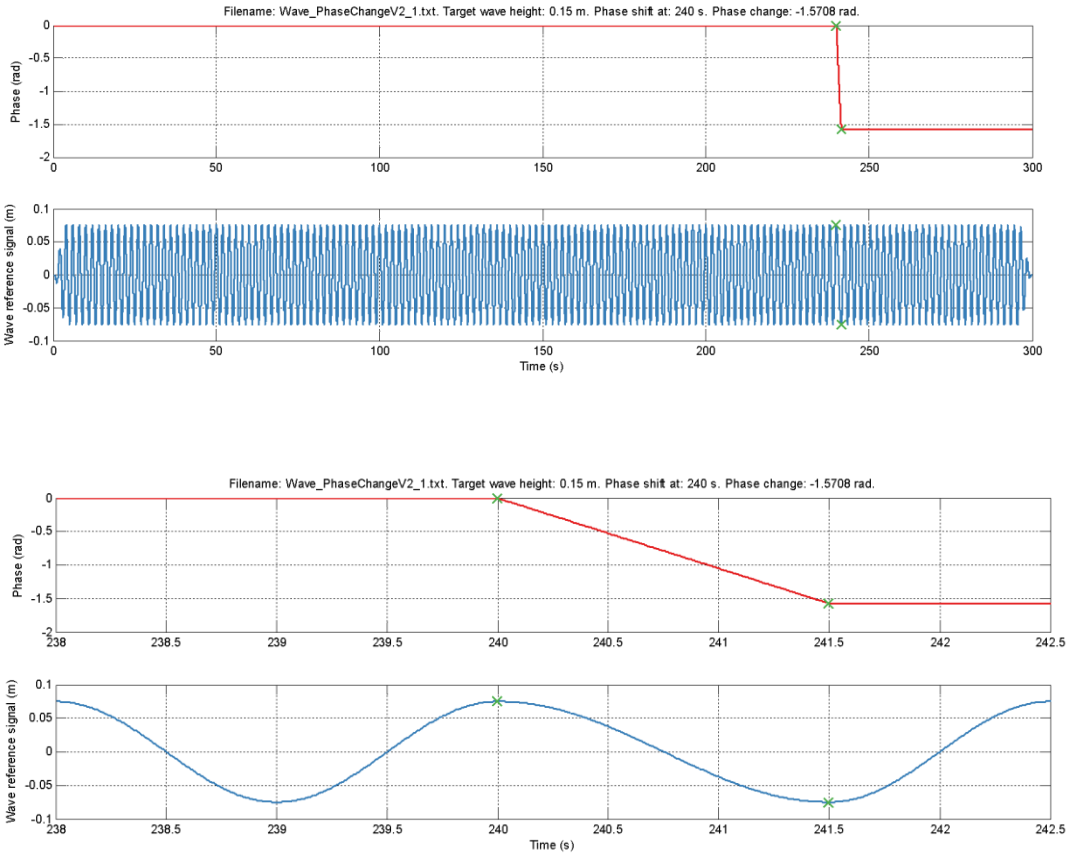

Figure 49 represents the phase shift type.

The figure below is showing the target wave for the positive phase shift.

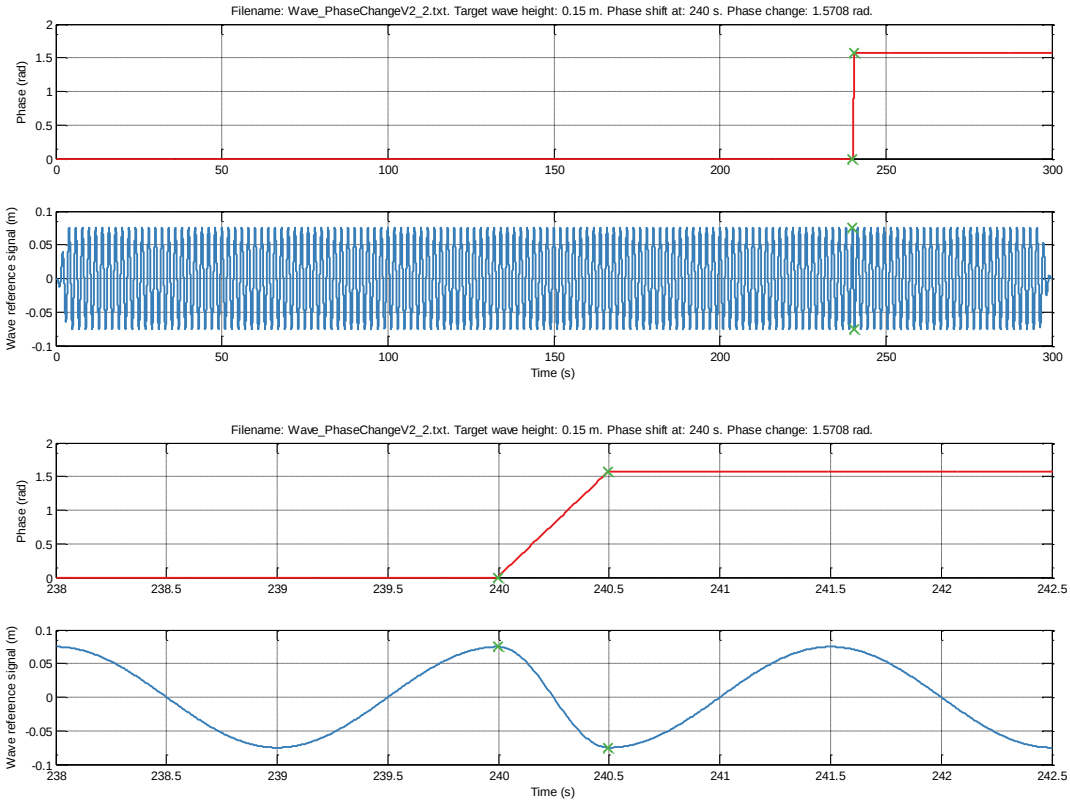

Figure 50 represents the target wave for the positive phase shift.

Appendix B: Measured wave time series and selection for analysis

In series J the device was not in the water, and the measured waves in these tests are therefore not influenced by the presence of the device in the water (e.g. reflections). The waves measured in series J has therefore been analysed in the following. The selection of the time for analysis has been chosen to be:

- Start at 15 seconds later than when the wave signal from WG1 is first exceeding 30 % of the max
- Stop at 5 seconds before than when the wave signal from WG1 is last exceeding 30 % of the max

In the following the selected part with all the WG-signals is shown on the upper graph and on the lower graph the first 5 seconds from the wave gauges in line with the absorber is shown.

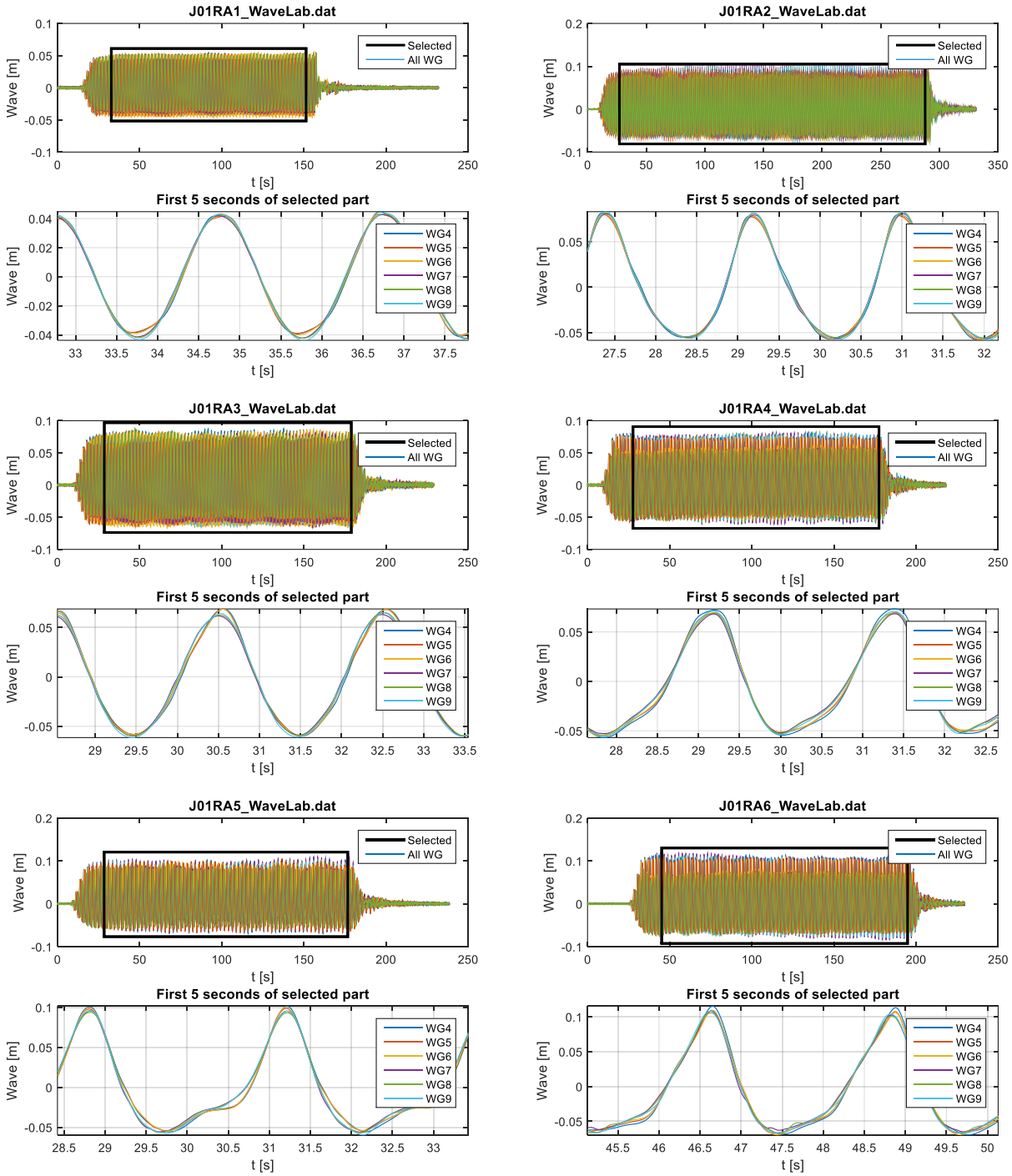

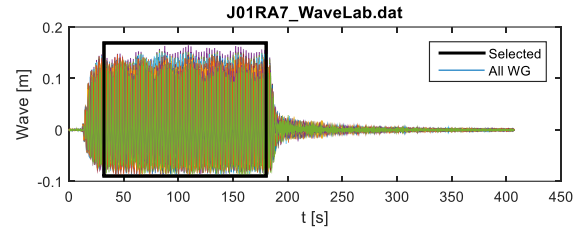
J01RA7_WaveLab.dat
Selected
All WG
Wave [m]
t [s]

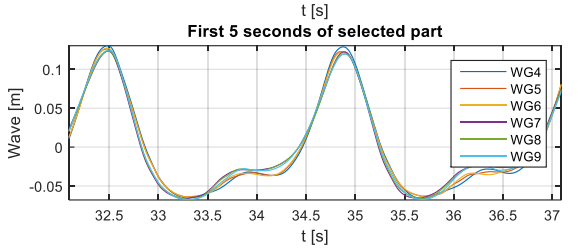
First 5 seconds of selected part
WG4
WG5
WG6
WG7
WG8
WG9
Wave [m]
t [s]

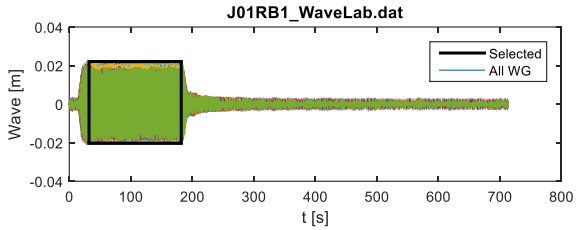
J01RB1_WaveLab.dat
Selected
All WG
Wave [m]
t [s]

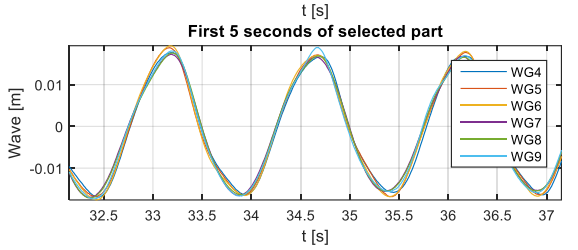
First 5 seconds of selected part
WG4
WG5
WG6
WG7
WG8
WG9
Wave [m]
t [s]

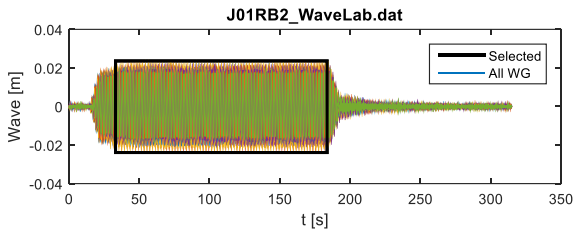
J01RB2_WaveLab.dat
Selected
All WG
Wave [m]
t [s]

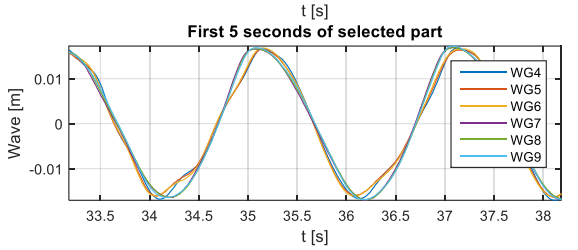
First 5 seconds of selected part
WG4
WG5
WG6
WG7
WG8
WG9
Wave [m]
t [s]

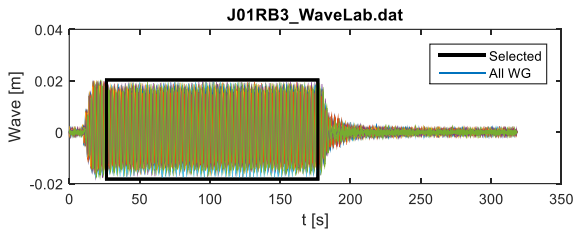
J01RB3_WaveLab.dat
Selected
All WG
Wave [m]
t [s]

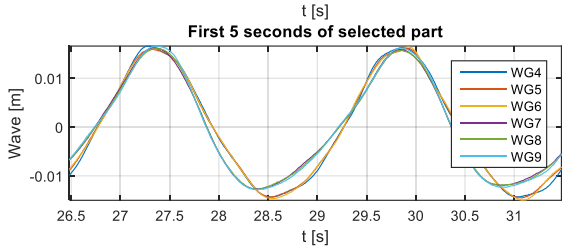
First 5 seconds of selected part
WG4
WG5
WG6
WG7
WG8
WG9
Wave [m]
t [s]

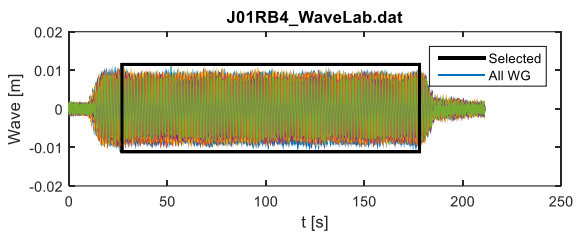
J01RB4_WaveLab.dat
Selected
All WG
Wave [m]
t [s]

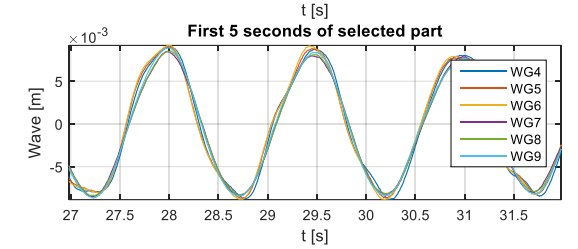
First 5 seconds of selected part
WG4
WG5
WG6
WG7
WG8
WG9
Wave [m]
t [s]

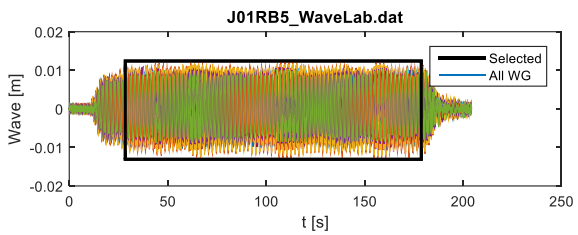
J01RB5_WaveLab.dat
Selected
All WG
Wave [m]
t [s]

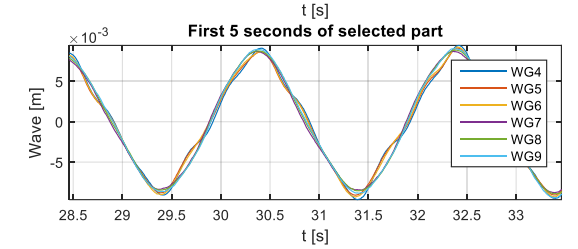
First 5 seconds of selected part
WG4
WG5
WG6
WG7
WG8
WG9
Wave [m]
t [s]

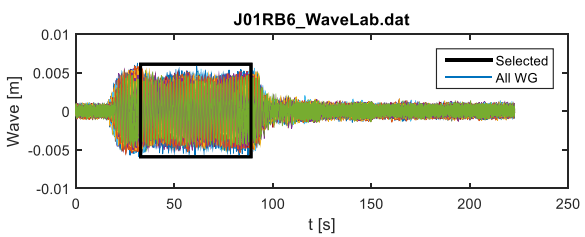
J01RB6_WaveLab.dat
Selected
All WG
Wave [m]
t [s]

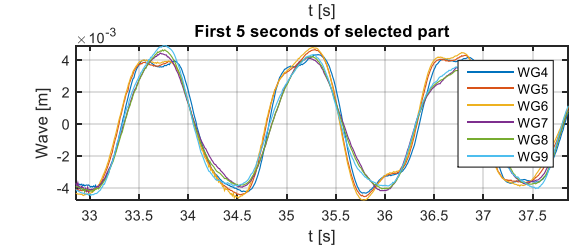
First 5 seconds of selected part
WG4
WG5
WG6
WG7
WG8
WG9
Wave [m]
t [s]

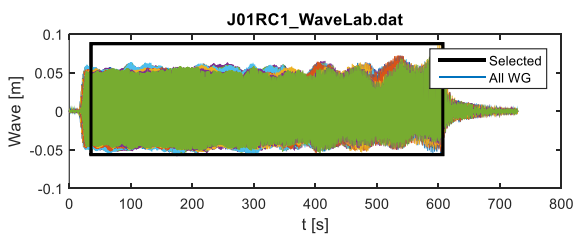
J01RC1_WaveLab.dat
Selected
All WG
Wave [m]
t [s]

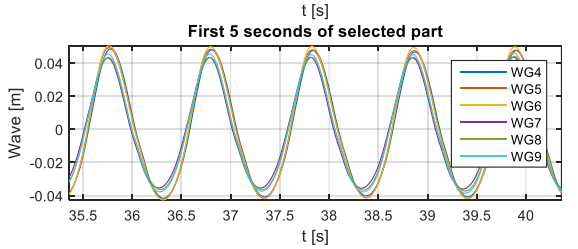
First 5 seconds of selected part
WG4
WG5
WG6
WG7
WG8
WG9
Wave [m]
t [s]

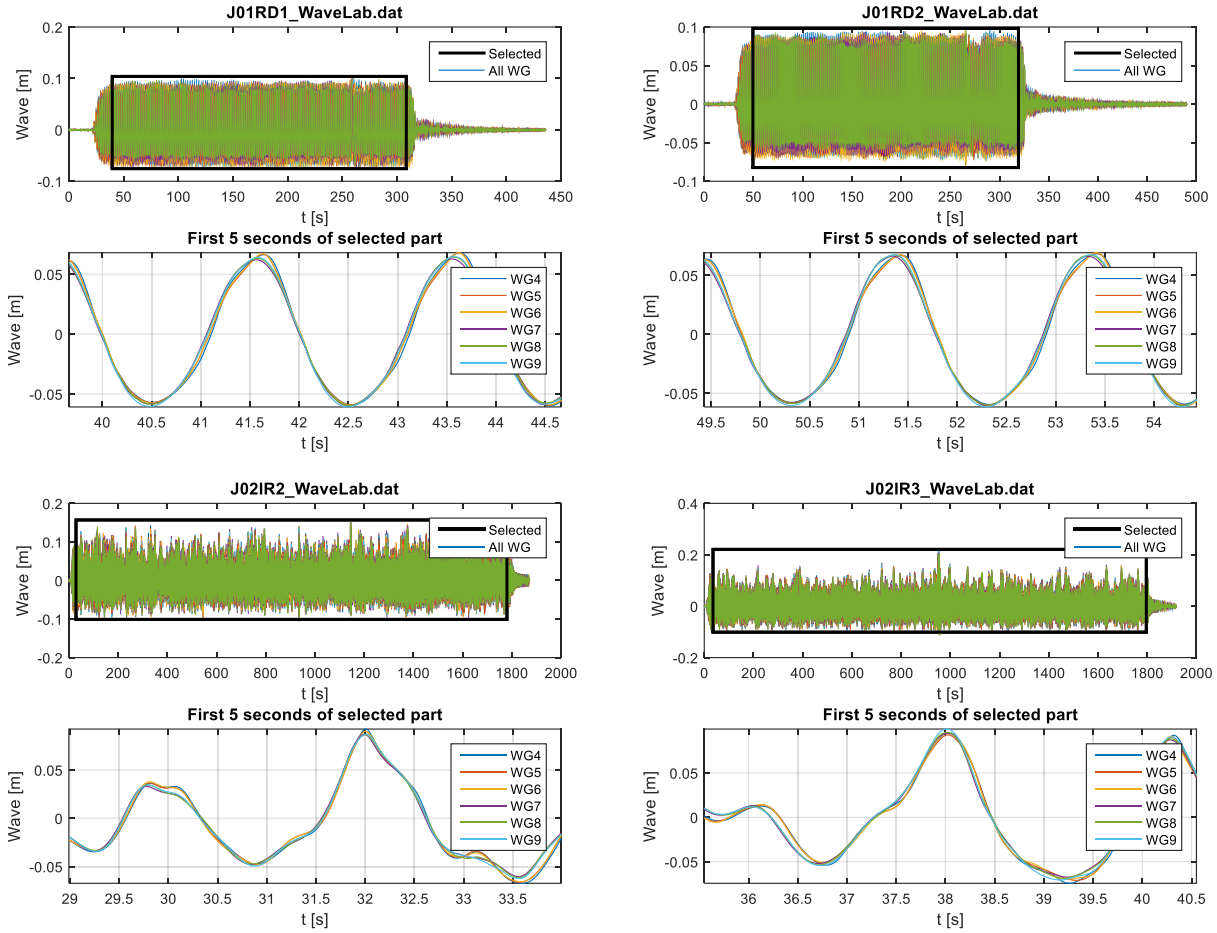

Figure 51 represents the wave time series with the period that is used for analysis.

Appendix C: Hydrodynamic and hydrostatic coefficients

The motion of the device is described in a coordinate system with origo located at the centre of the arm bearing. Waves are propagating in the direction of the x-axis.

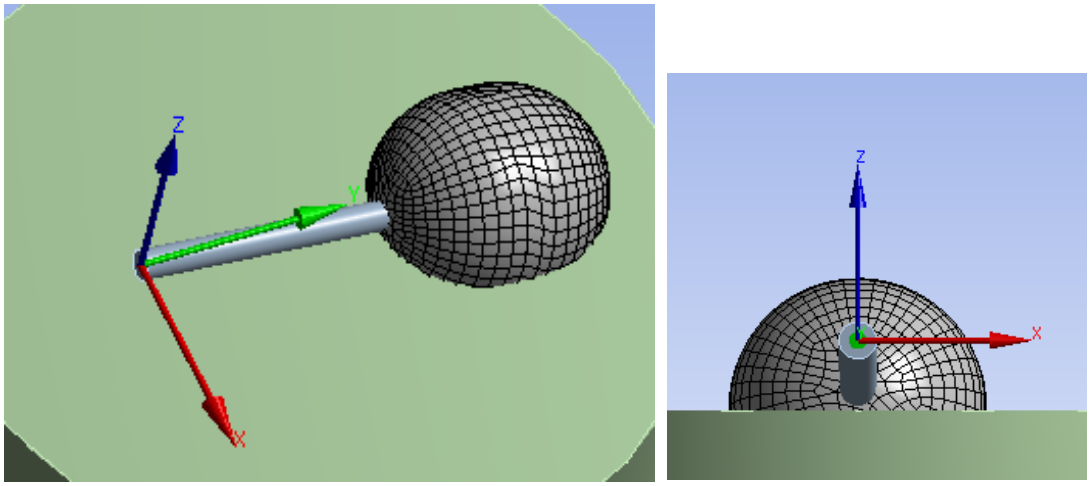

Figure 52 represents the coordinate system for the motions.

The motion of the ball is described with standard sign convention for right-handed coordinate systems as shown in

.

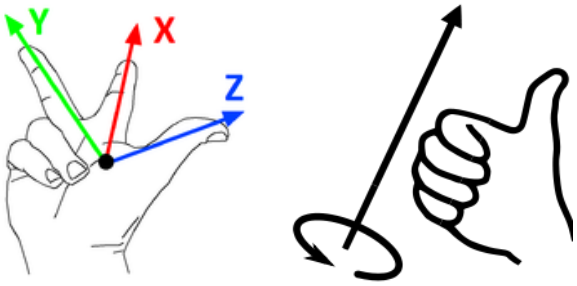

Figure 53. Standard sign convention for right-handed coordinate systems. [http://en.wikipedia.org/wiki/Right-hand_rule].

The signs for the two outer degrees of freedom is shown in Figure 34.

Roll, φ

Seen from the side

Yaw, θ

Seen from above

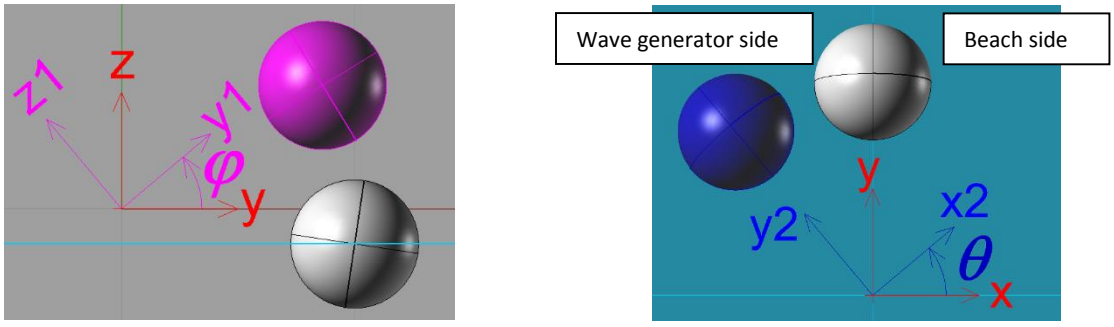

Figure 54. Sign for the two external degrees of freedom φ and θ.

Description of coefficients

The method used to describe the hydrodynamics by linear superposition is the traditional way it is usually done. The method is described in most hydrodynamic textbooks such as the book by Falnes (2003) and Faltinsen (1993). Another alternative which is highly recommendable is the WAMIT manual, which can be downloaded from the Internet for free. The equation of motion is described by three second order differential equations:

1) Roll: $J_\varphi \ddot{\varphi} + "More" = M_{d\varphi} - M_{g\varphi} \Rightarrow J_\varphi \ddot{\varphi} + "More" = M_{e\varphi} + M_{r\varphi} + M_{h\varphi}$

2) Yaw: $J_\theta \ddot{\theta} + "More" = M_{d\theta} \Rightarrow J_\theta \ddot{\theta} + "More" = M_{e\theta} + M_{r\theta}$

3) Flywheel: $J_\alpha \ddot{\alpha} + "More" = M_c$

J: Mass inertia moment of the moving body

M_d: Hydrodynamic moment (from water pressure on hull)

M_g: Gravitational moment

M_c: Control moment from Power Take Off

M_h: Hydrostatic moment, $M_{h\varphi} = -k_{h\varphi}\varphi$

M_r: Radiation moment, $M_{r\varphi} = -m_{\infty\varphi}\ddot{\varphi} - M_{r\varphi,conv}$, $M_{r\varphi,conv} = \int_{-\infty}^{t} k_{r\varphi}(t-\tau)\dot{\varphi}\,(\tau)d\tau$

$M_{r\theta} = -m_{\infty\theta}\ddot{\theta} - M_{r\theta,conv}$, $M_{r\theta,conv} = \int_{-\infty}^{t} k_{r\theta}(t-\tau)\dot{\theta}\,(\tau)d\tau$

M_e: Wave excitation moment, $M_{e\varphi} = \int_{-\infty}^{\infty} h_{e\varphi}(t-\tau)\eta\,(\tau)d\tau$, $M_{e\theta} = \int_{-\infty}^{\infty} h_{e\theta}(t-\tau)\eta\,(\tau)d\tau$

Notes:

- The "More" term is described in Nielsen et al. (2015). This part include the dynamic interaction between the flywheel and the body motion.
- The gravity moment and the hydrostatic moment is zero for yaw (this is always the case as the z-axis by definition is vertical)
- There is no hydrodynamic interaction between motion in yaw and roll, i.e. off-diagonal terms in the hydrodynamic radiation matrix is zero.

Element model

The element model of the float surface is constructed in the CAD program Rhinoceros and exported to WAMIT, see Figure 35.

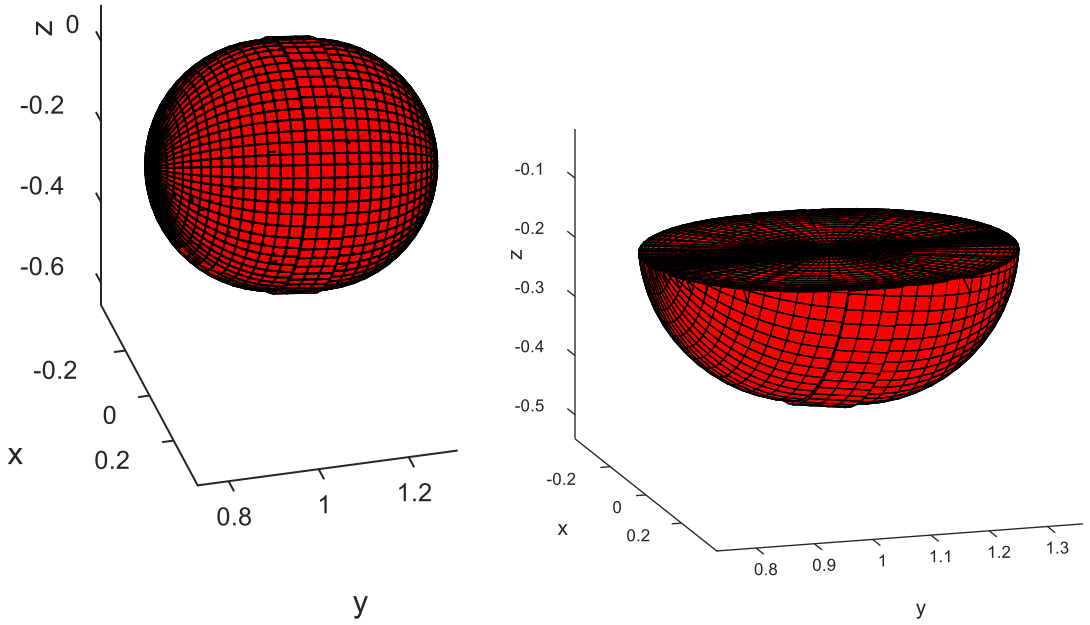

Figure 55. Element model of float. Full part of ball (left) and the submerged part used for WAMIT (right).

The volume of the submerged part is 0.04633 m^3 corresponding to a displaced mass of 46.3 kg. The Center of Buoyancy is at (Xb,Yb,Zb) = (0, 1.050, -0.246) m.

Hydrostatics

The linear hydrostatics is found by WAMIT (numerical) estimation for the approximate geometry:

$k_{h\varphi}$ **= 2925 Nm/rad**

The non-linear hydrostatics is calculated in Excel sheet. The results are confirmed by measurements.

Table 31 presents the hydrostatic moment

Absolute rotation (°)	Absolute rotation (rad)	φ (rad)	Hydrostatic moment (Nm)
7	0.122	0.246	-479.68
6	0.105	0.229	-477.85
5	0.087	0.211	-469.15
4	0.070	0.194	-453.84
3	0.052	0.176	-432.50
2	0.035	0.159	-405.69
1	0.017	0.142	-373.94
0	0.000	0.124	-337.75
-1	-0.017	0.107	-297.69
-2	-0.035	0.089	-254.27
-3	-0.052	0.072	-208.04
-4	-0.070	0.054	-159.55
-5	-0.087	0.037	-109.33
-6	-0.105	0.019	-57.93
-7	-0.122	0.002	-5.89
-7.112	-0.124	0.000	-0.04
-8	-0.140	-0.015	46.28
-9	-0.157	-0.033	98.05
-10	-0.175	-0.050	148.91
-11	-0.192	-0.068	198.37
-12	-0.209	-0.085	245.98
-13	-0.227	-0.103	291.27
-14	-0.244	-0.120	333.82
-15	-0.262	-0.138	373.22
-16	-0.279	-0.155	409.11
-18	-0.314	-0.190	469.01
-20	-0.349	-0.225	511.22
-22	-0.384	-0.260	534.59
-24	-0.419	-0.295	539.56
-25	-0.436	-0.312	535.98

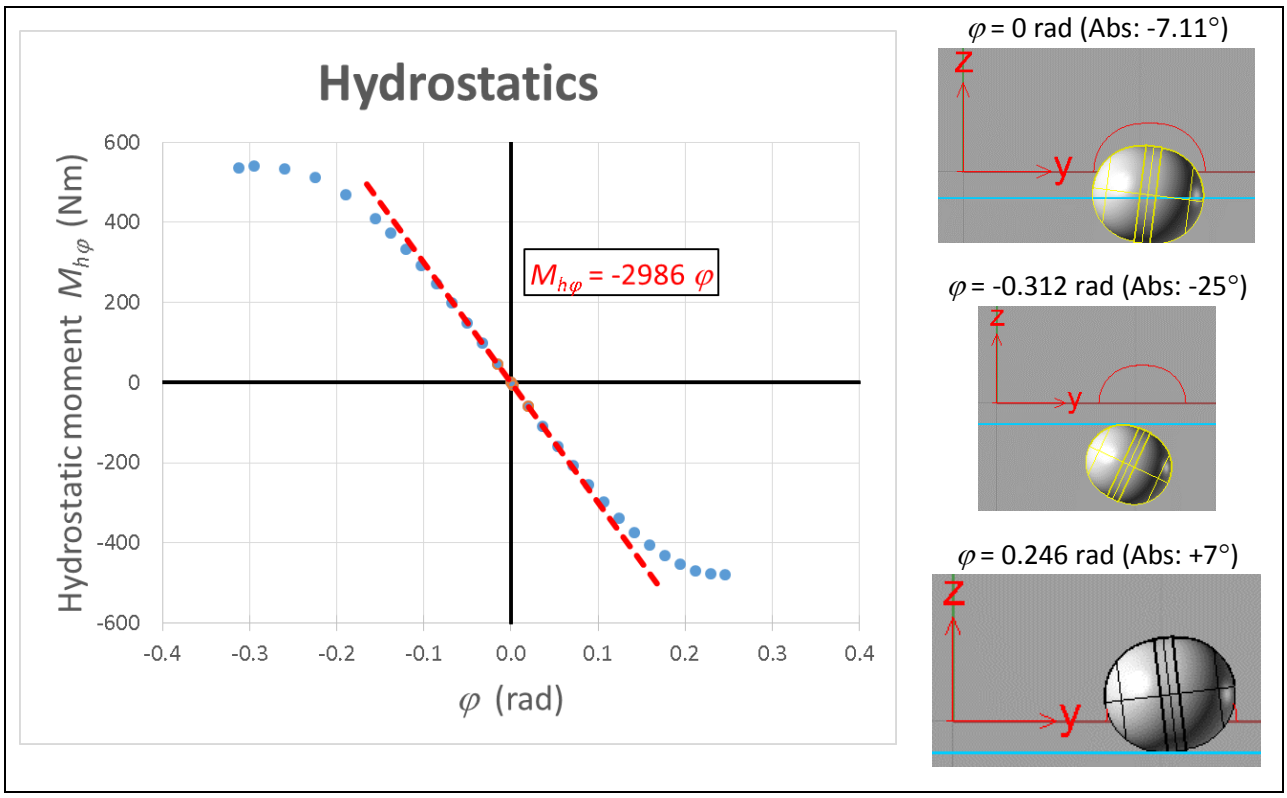

Figure 56. Non-linear and linear hydrostatics calculated from the exact geometry.

Hydrodynamic added mass and damping

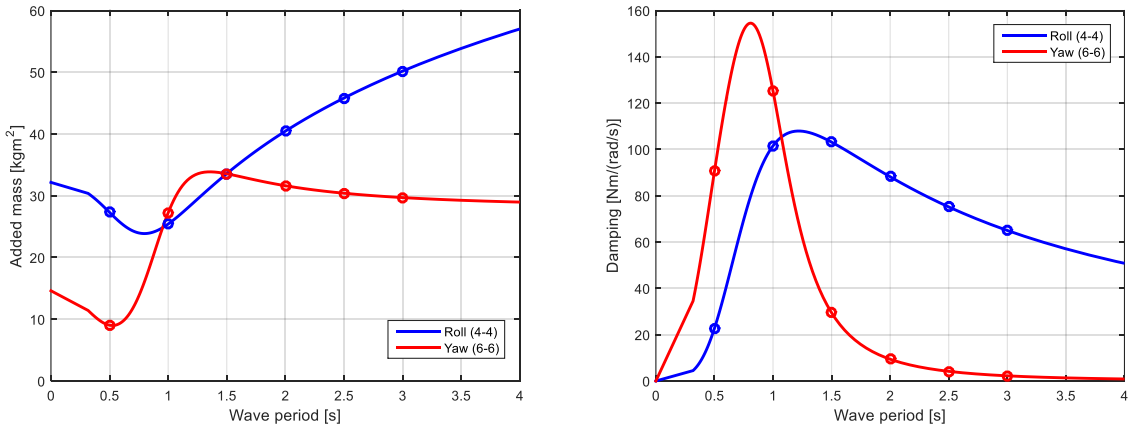

Figure 57. Wave radiation in frequency domain, added mass (left) and damping (right). Calculated by WAMIT.

Hydrodynamic wave force

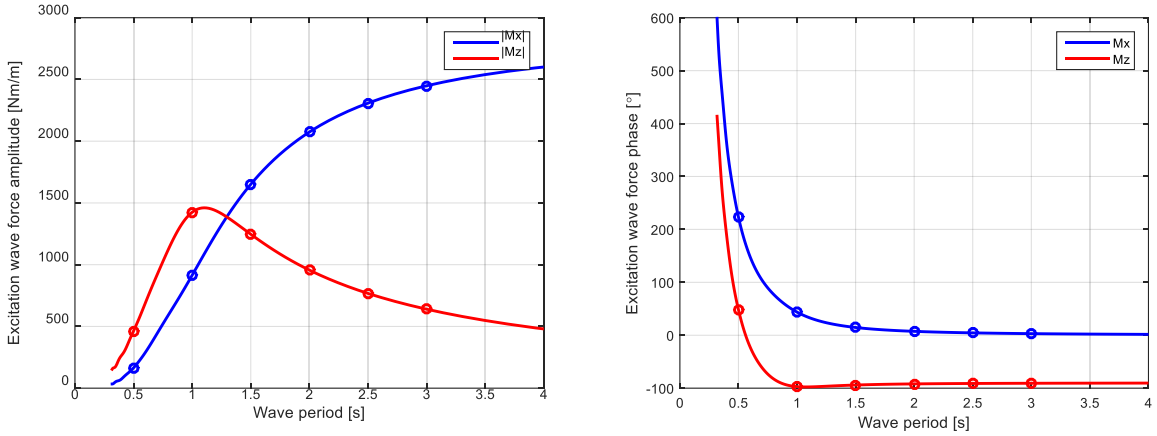

Figure 58. Wave excitation in frequency domain, amplitude (left) and phase (right). Calculated by WAMIT.

Phases are defined according to Figure 59.

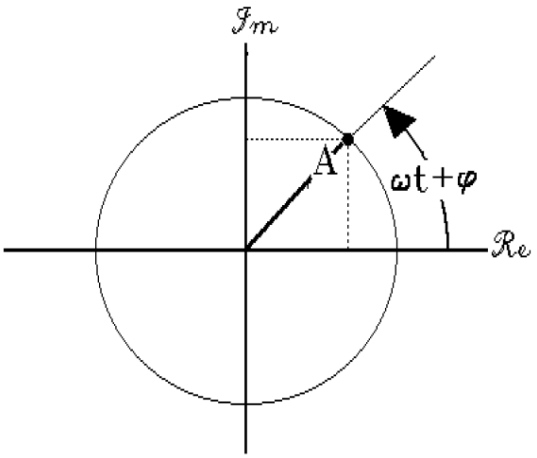

$$Signal(t) = Re(Ae^{i\omega t}) = |A|cos(\omega t + \varphi)$$

Figure 59. Definition of phases.

Tabulated data

Water depth: 0.60 m.

Water density: 1000 kg/m^3.

Gravity: 9.82 m/s^2.

Hydrostatic stiffness coefficient: $k_{h\varphi}$ = 2925 Nm/rad (for vertical motion of the ball)

Mooring stiffness coefficient: $k_{s\theta}$ = 149 Nm/rad (for horizontal motion of the ball)

Table 32. Hydrodynamic coefficients.

Period	Wave radiation				Wave excitation			
T [s]	$C_{h,44}$ [Nm/(rad/s)]	$C_{h,66}$ [Nm/(rad/s)]	$J_{h,44}$ [kgm^2]	$J_{h,66}$ [kgm^2]	M_x [Nm/m]	M_x [°]	M_z [Nm/m]	M_z [°]
0.5	22.76	90.56	27.30	9.04	164.7	223.3	463.1	48.3
1.0	101.55	125.20	25.42	27.23	914.5	43.7	1424.4	-97.1
1.5	103.15	29.46	33.58	33.56	1650.9	14.7	1246.7	-94.0
2.0	88.20	9.40	40.46	31.62	2074.0	7.4	956.4	-91.9
2.5	75.17	4.16	45.82	30.41	2308.3	4.5	767.5	-91.1
3.0	65.01	2.22	50.19	29.70	2448.8	3.1	639.7	-90.7

Wave radiation coefficients:

- 44-coefficients are for "roll motion", rotation about x, i.e. vertical displacement of the ball.
- 66-coefficients are for "yaw motion", rotation about z, i.e. horizontal motion of the ball

Wave excitation coefficients:

- Moment amplitudes in [Nm/m] must be multiplied by the wave amplitude in [m] to give the actual moment amplitude in [Nm].
- Moment phases are given relative to wave input at the centre of the absorber, i.e. at x = 0.
- Mx is the moment about the x-axis, i.e. the moment that pushes the float upwards.
- Mz is the moment about the z-axis, i.e. the moment that pushes the float towards the wave generator

WAMIT 6 dof hydrodynamic parameters in frequency domain

Added mass and damping

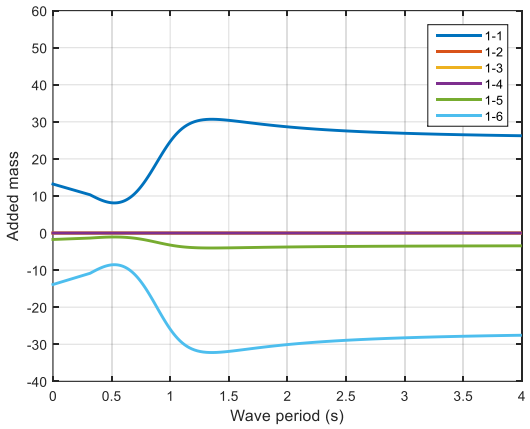

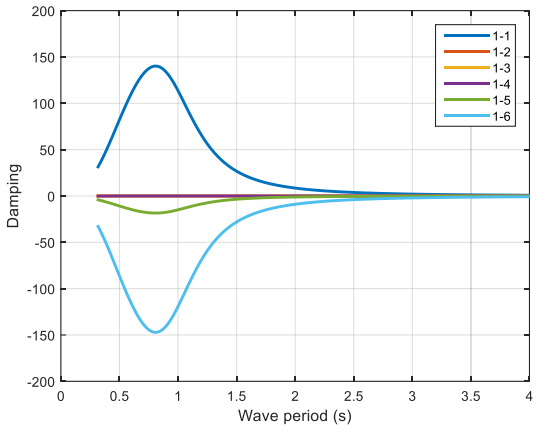

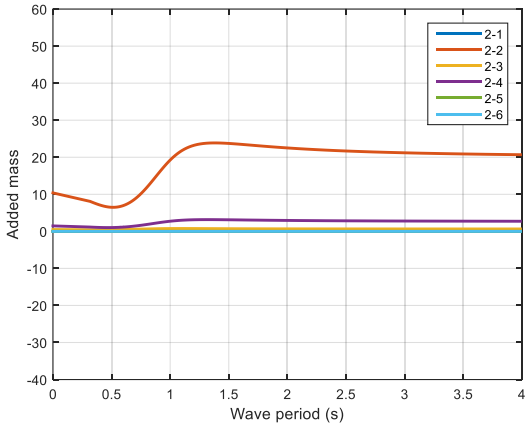

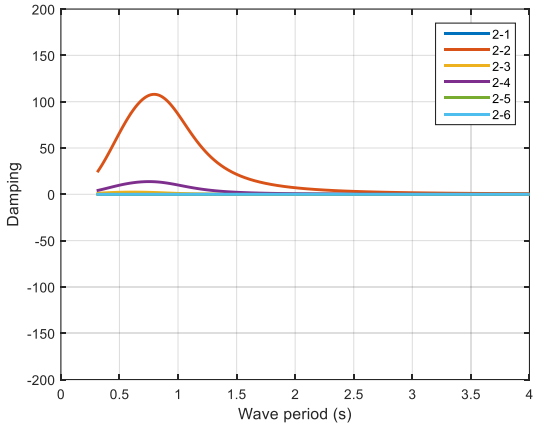

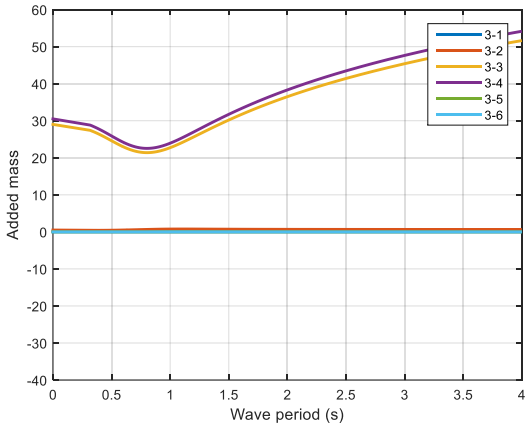

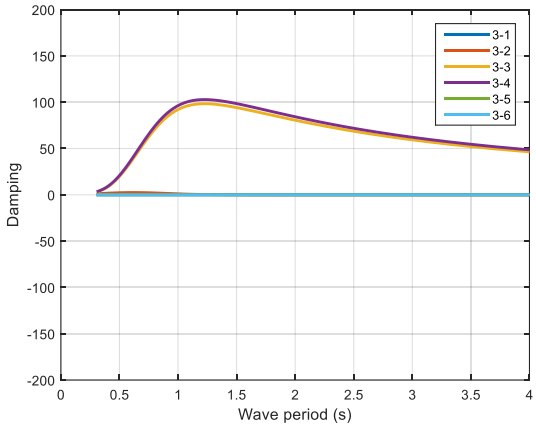

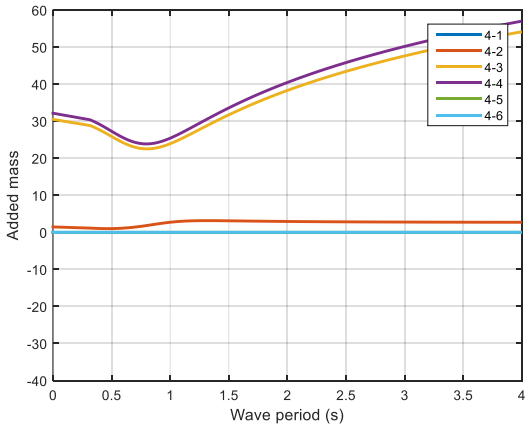

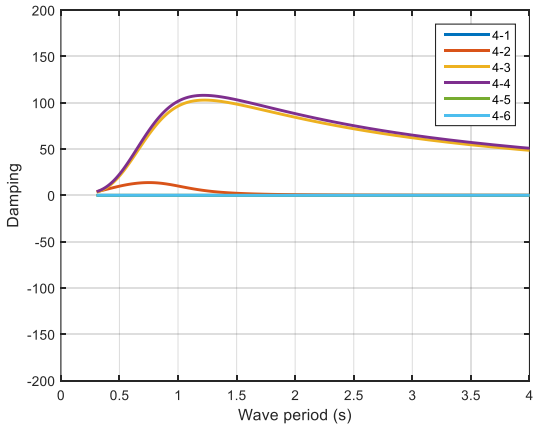

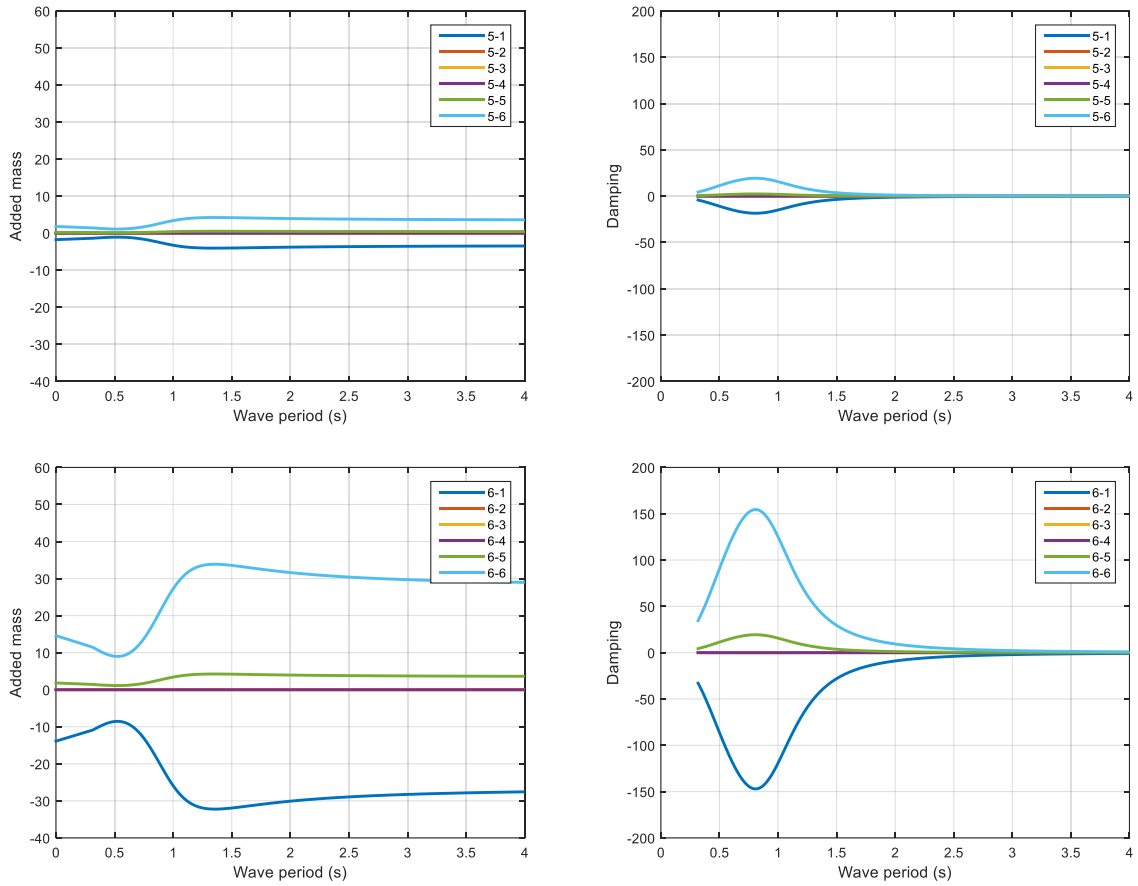

Figure 60 presents the results from WAMIT in terms of added mass and damping

Wave force

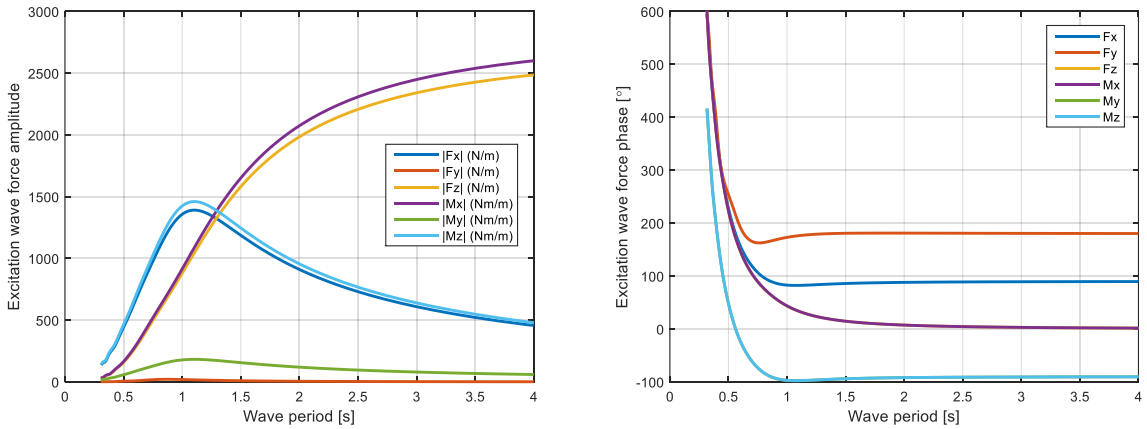

Figure 61 presents the results from WAMIT in terms of wave force

ISSN 1901-726X

DCE Technical Report No. 178